Innovations Deserving Exploratory Analysis Programs

IDEA

FIELD EVALUATION OF BALLAST FOULING CONDITIONS USING MACHINE VISION

IDEA Program Final Revised Report

Contract Number: SAFETY-27

Prepared for the IDEA Program
Transportation Research Board
The National Academies

Principal Investigator: Erol Tutumluer, Ph.D.
Key Investigators: Narendra Ahuja, Ph.D. and John M. Hart
Postdoctoral Research Associate: Maziar Moaveni, Ph.D.
Research Assistants: Haohang Huang, Zixu Zhao and Sagar Shah

University of Illinois at Urbana-Champaign

Submittal Date: October 2017

Innovations Deserving Exploratory Analysis (IDEA) Programs Managed by the Transportation Research Board

This IDEA project was funded by the Rail Safety IDEA Program. The TRB currently manages the following three IDEA programs:

- The NCHRP IDEA Program, which focuses on advances in the design, construction, and maintenance of highway systems, is funded by American Association of State Highway and Transportation Officials (AASHTO) as part of the National Cooperative Highway Research Program (NCHRP).
- The Rail Safety IDEA Program currently focuses on innovative approaches for improving railroad safety or performance. The program is currently funded by the Federal Railroad Administration (FRA). The program was previously jointly funded by the Federal Motor Carrier Safety Administration (FMCSA) and the FRA.
- The Transit IDEA Program, which supports development and testing of innovative concepts and methods for advancing transit practice, is funded by the Federal Transit Administration (FTA) as part of the Transit Cooperative Research Program (TCRP).

Management of the three IDEA programs is coordinated to promote the development and testing of innovative concepts, methods, and technologies.

For information on the IDEA programs, check the IDEA website (www.trb.org/idea). For questions, contact the IDEA programs office by telephone at (202) 334-3310.

IDEA Programs Transportation Research Board 500 Fifth Street, NW Washington, DC 20001

ACKNOWLEDGEMENTS

The authors of this report would like to acknowledge the support for this research provided by the Association of American Railroads (AAR) as part of technology outreach research program. Particularly the great contributions by David Davis and Mike McHenry, who provided ballast trench samples and transversal cross section ballast imaging opportunities at Transportation Technology Center (TTC) in Pueblo, CO is appreciated. Many thanks are also due to Union Pacific Railroad and Dr. Samuel C. Douglas, former manager of special projects, for the ballast box study samples utilized from the western Heavy Axle Load (HAL) revenue service test mega-site in Ogallala, NE.

The authors would like to acknowledge the guidance and research support from Dennis Morgart, William (Zach) Dombrow, and Mike Wnek of BNSF Railway, which provided additional gift funds in support of research activities including track access, excavation equipment, and the coordination during shoulder ballast imaging field applications on BNSF lines near Kansas City, MO.

Moreover, the authors highly appreciate the great help and support that was provided by Dennis Mathison, Ken Range, and John Hembery of Loram Maintenance of Way during the ballast field imaging trip in Martinton, IL. This includes providing safe access to an active Shoulder Ballast Cleaning (SBC) project site, assistance during image acquisition from exposed shoulder ballast cross sections as well as giving us very useful information about technical and operational specifications of different models of SBC equipment.

The assistance from several graduate research assistants including Shengnan Wang and Xing Li from the Computer Vision and Robotics Laboratory (CVRL) in the Beckman Institute for Advanced Science and Technology at the University of Illinois at Urbana-Champaign (UIUC) for their contributions in the development of image processing algorithms and establishment of the graphical user interface is greatly appreciated. Additionally, the assistance from Issam Qamhia, graduate research assistant, and Yifeng Chu, undergraduate research assistant, during laboratory ballast imaging in CVRL is appreciated. Many thanks go to the staff and research engineers at the Illinois Center for Transportation (ICT) housed in the Advanced Transportation Research Engineering Laboratory (ATREL) as well as machine shops in both Civil and Environmental Engineering and Electrical and Computer Engineering departments at UIUC for their assistance in different stages of this project.

Finally, the authors would like to recognize the great contributions and useful comments provided by the members of Safety IDEA program committee including Ms. Jo Allen Gause as this IDEA project's Program Manager and the Safety-27 project's expert review panel, who helped to improve the quality of the contents of this report. The expert review panel consisted of Gary Carr with Federal Railroad Administration (FRA), Dennis Morgart and Hank Lees (retired) with BNSF, Brad Kerchof with Norfolk Southern (NS), Dennis Mathison with Loram Maintenance of Way and finally, Conrad Ruppert with RailTEC at UIUC.

The contents of this report reflect the views of the authors who are responsible for the facts and the accuracy of the data presented herein. This report does not constitute a standard, specification, or regulation.

TABLE OF CONTENTS

EXECUTIVE SUMMARY

This research project introduces a machine vision-based inspection system to assess ballast degradation levels in field setting. This system incorporates an approach to ballast sampling, procedures for image acquisition of horizontal and vertical ballast cross sections, and proposes an image based index called "Percent Degraded Segments" (PDS) and defined in terms of image segments. These segments are regions extracted by an image segmentation process and correspond to ballast pieces or parts thereof. Our system's performance was validated using a variety of ground truth data. A Graphical User Interface (GUI) was developed to assist users in processing the acquired images and finding the best segmentation parameters. Finally, a statistical approach was used to relate PDS and the commonly used Selig's Fouling Index (FI) through regression analysis.

Figure 1 summarizes our approach, which provides a method of continuous evaluation of degradation levels along the track that can help decision makers and track inspectors to select efficient ballast maintenance and rehabilitation strategies to achieve targeted levels of track performance.

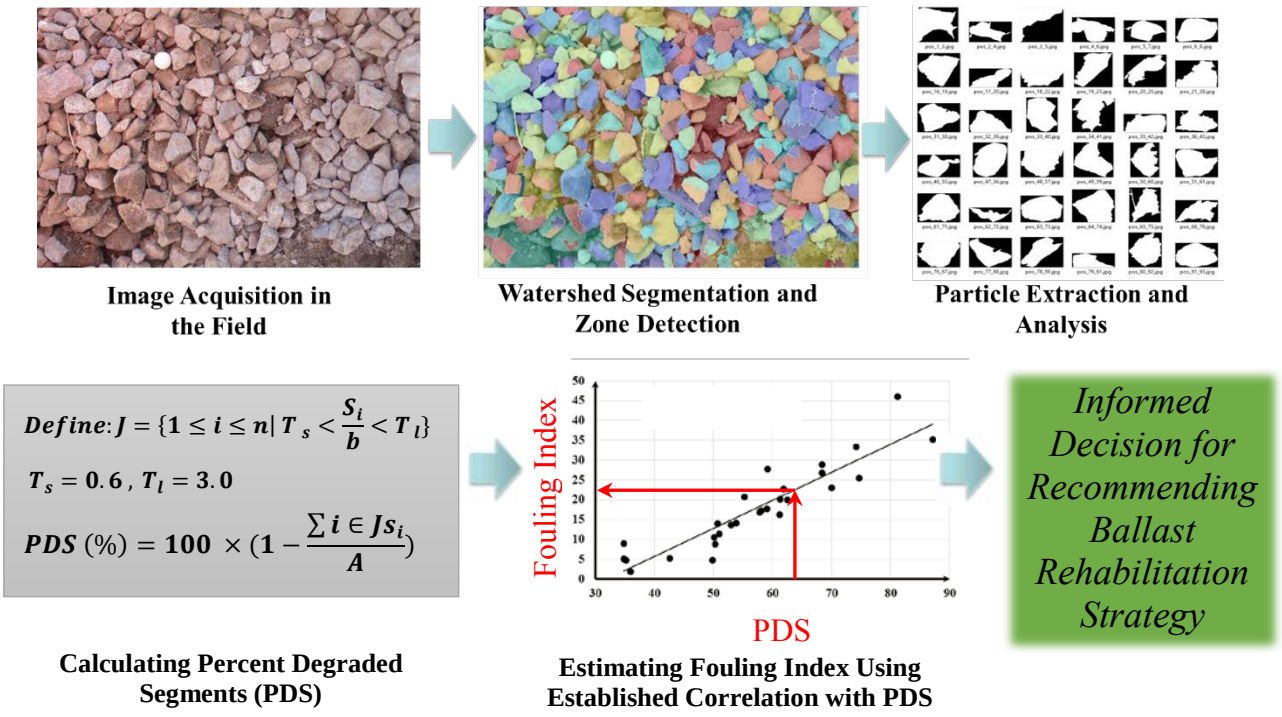

FIGURE 1. Our method for estimating ballast degradation using the proposed PDS index

Stage 1 of this IDEA project included database development, algorithm development as well as laboratory and field imaging. A comprehensive database including ballast cross section images at different degradation levels was created in the laboratory by manufacturing a custom designed ballast imaging tray. These data were input to our machine vision algorithm for functional testing. Further analysis confirmed the need for collecting actual images from the field where the system must perform. Therefore, field images were captured on a test track at Transportation Technology Center (TTC) facility in Pueblo, CO. The resulting field images were combined with more data obtained from a novel ballast sampling method to produce an improved image processing algorithm. Finally, corresponding FI values obtained through sieve analysis of the samples were used to validate the machine vision algorithm and to further improve performance.

Stage 2 of this IDEA project included application of the PDS approach to images obtained from Shoulder Ballast Cleaners (SBC) during routine maintenance operations. The research team visited an active shoulder ballast cleaning project site on Union Pacific track in Martinton, Illinois. Shoulder ballast's horizontal cross sectional images generated by the SBC 15 equipment were collected at two different locations in addition to their corresponding ballast samples. Subsequently, a second imaging trip was organized with BNSF Railway to visit several in-service track sites near Kansas City, MO. Twelve horizontal shoulder ballast cross section images at different degradation levels and ballast samples for laboratory validation

were collected. Image analysis verified our methodology for classifying ballast images based on severity of degradation found by the PDS method.

A regression analysis model with a high coefficient of determination (R^2= 0.84) was established. Although limited field data were collected in this study, a strong relationship between FI and PDS showed that FI values can be reliably estimated from PDS results. Furthermore, the PDS index can be used for development of a robust Imaging Based Fouling Index (IBFI) for future applications to spot checking and eventual improvements in maintenance.

This technology can be installed on current and future generations of SBC equipment to automate the evaluation of ballast condition from images of the cut shoulders below the ties. This automated evaluation could greatly improve the quality and efficiency of inspections. In the longer term, SBC equipment would become a continuous data collection device for automatic ballast inspection. In addition, the results of this process could be used to map out recommendations of follow-up rehabilitation strategies to address any safety concerns related to ballast degradation. The proposed method has the potential to be applied for in-situ evaluation of permeability and strength properties of railroad ballast at different degradation levels. Such a system should be considered as a component of a comprehensive Ballast Management System (BMS) to help better understand deterioration mechanisms and improve ballasted track designs, inspection, and maintenance practices. This will provide predictive service life and life cycle analysis for improving the safety and network reliability of US railroad transportation system.

1. IDEA PRODUCT

The current methods for evaluating the level of ballast degradation for an in-service track include sampling and mechanical sieve analysis or visual inspection by track inspectors. Ballast sampling and sieving are costly, labor intensive and time-consuming processes. Furthermore, visual inspections are highly dependent on the level of track inspector's expertise and hence very subjective. Finally, the locations along the track where ballast samples are obtained can introduce extreme variability in the reported degradation levels.

1.1. MACHINE VISION BASED BALLAST DEGRADATION EVALUATION

The IDEA product is a machine vision approach for performing ballast inspection continuously along the track. This technique utilizes an innovative degradation index called Percent Degraded Segments (PDS) based on image analysis for quantifying the level of ballast degradation in the field, without the need for ballast sampling and sieving operations. Machine vision algorithms are implemented to process the images of horizontal and vertical ballast cross sections. This technology can efficiently quantify ballast fouling levels and potentially replace the current state-of-the-practice of visual inspection, sampling, and mechanical sieve analysis. The process of this IDEA product is shown in Figure 2.

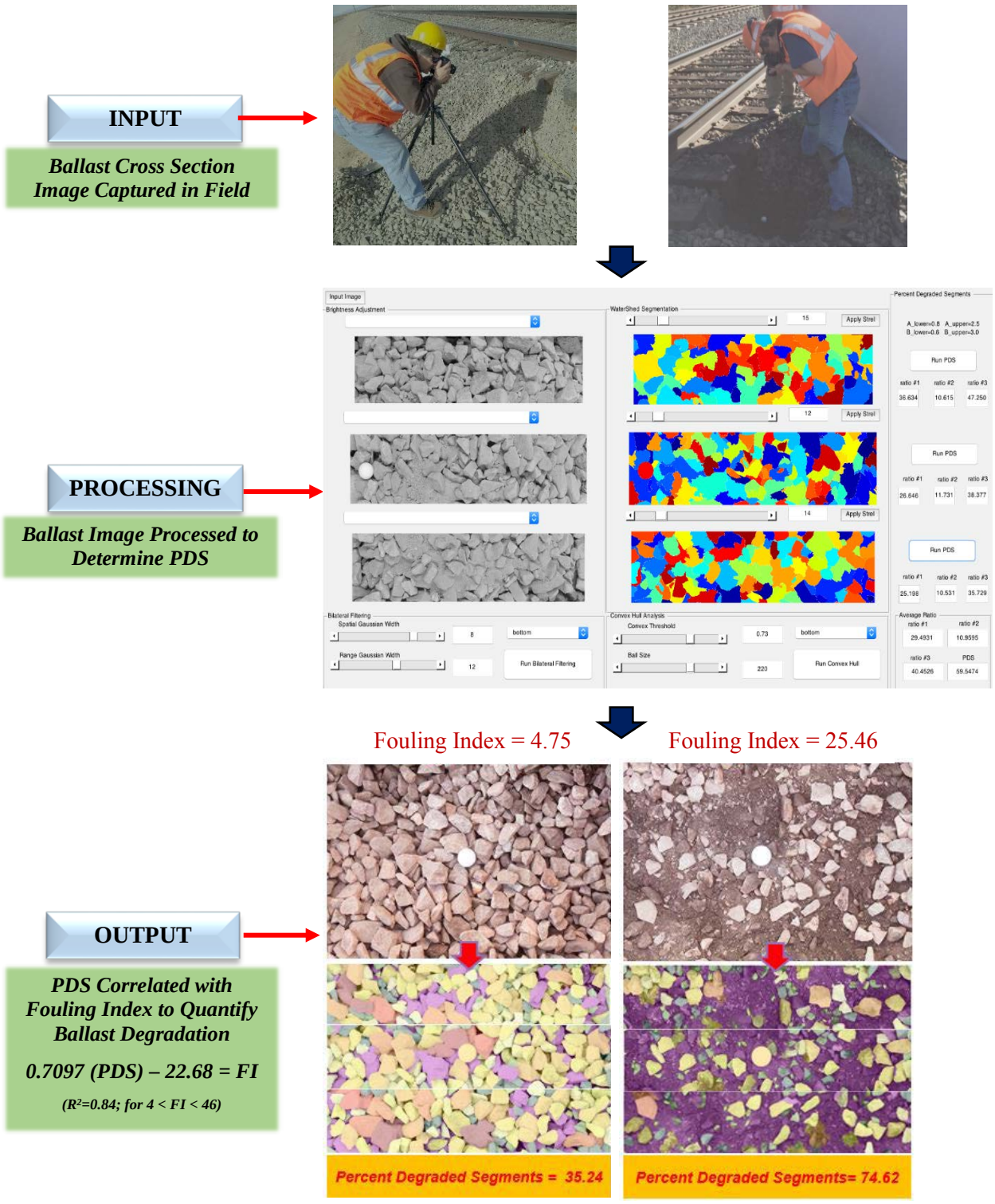

FIGURE 2. IDEA Product - Machine Vision Ballast Inspection System (MV-BIS)

2. CONCEPT AND INNOVATION

We have developed a new technology for on-site characterization of railroad ballast, using visual spectrum sensing via machine vision techniques, for determining ballast quality evaluation and fouling condition assessment. An innovative image-based index, Percent Degraded Segments (PDS), has been established through laboratory and field research experimentation. This technology provides the capability for on-site quantification of ballast degradation trends in the field with a reliable, fast and semi-automated machine vision-based algorithm. To make available meaningful degradation levels for researchers, practitioners, and track inspectors, the new PDS index has been correlated to the commonly used Selig's Fouling Index (FI) based on the sieve analyses of ballast samples.

Current approaches for determining ballast condition based on visual inspection of the track are mostly qualitative and subjective in nature. In addition, when a problematic track site is encountered and degraded ballast is suspected as the cause, a proper quantification of the ballast fouling is done using Selig's FI. This requires tedious ballast sampling work with its inherent difficulties related to sample location/depth (spatial), sample size variability, and time-consuming mechanical sieving which is performed in the laboratory. In contrast, our custom machine vision inspection approach provides continuous and on-track quantification of ballast fouling conditions.

Our approach uses computer vision algorithms running on a laptop for processing high resolution digital images of ballast cross sections acquired in the field. We propose an "image with corresponding sample" method for field ballast sampling and acquiring ballast pieces that appear in the acquired image. We can thus compare and validate the results of our computer vision algorithm with the original Selig's FI values determined as ground truth for that location, by *shaving off* the representative sample from the cross section and using the existing sieving methods.

A new procedure was developed to acquire images of horizontal cross sections of ballast in the shoulder. Horizontal cross sections are more stable than vertical ones, which is especially relevant for SBC operations (see Figure 3). Therefore, the images of these cross sections can be continuously captured by a camera mounted on an SBC. Furthermore, horizontal ballast cross section imaging also provides an opportunity to quantify degradation at different depths of the ballast layer. Horizontal imaging can also enable SBC equipment to obtain degradation quantification at a desired cutting depth. We envision a further methodology, based on horizontal imaging, to enable ballast remediation procedures for railroads to determine the extent of shoulder cleaning required. These can then be integrated into shoulder ballast cleaning operations.

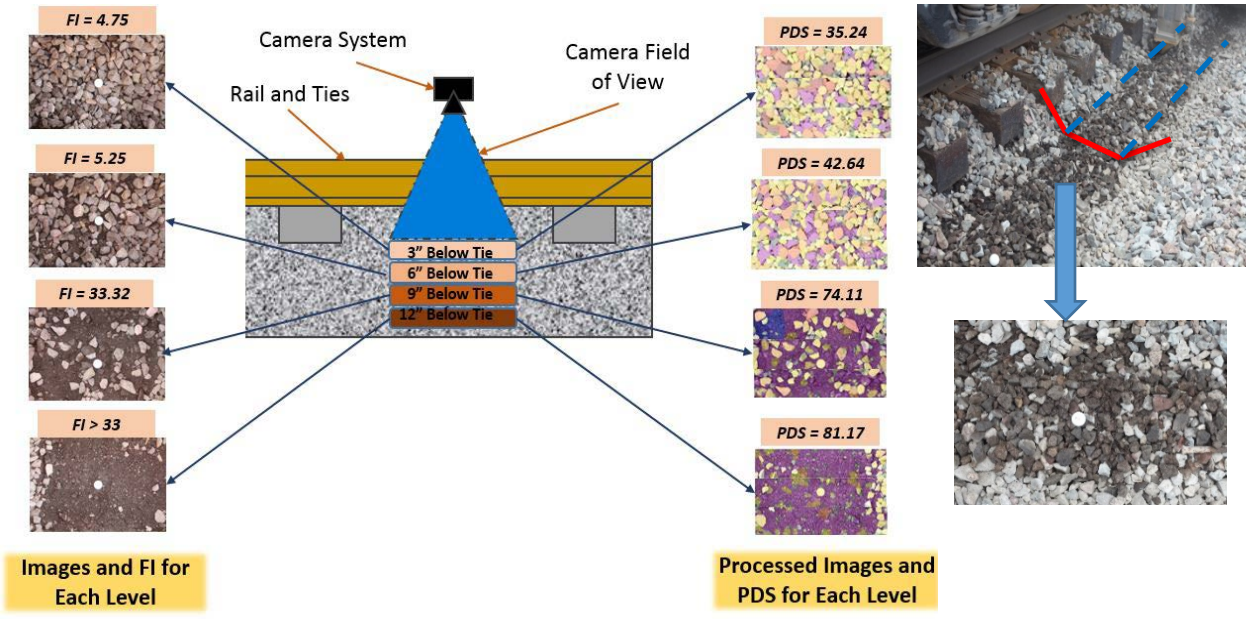

FIGURE 3. A proposed horizontal imaging method for determining level of ballast degradation at various depths (left) – Undisturbed horizontal cross section generated by shoulder ballast cleaners (right)

3. INVESTIGATION

Railroad ballast is uniformly-graded coarse aggregate placed between and immediately underneath the crossties to provide drainage and structural support for the repeated loading applied by train traffic. As ballast ages, it is progressively subjected to degradation caused by particle breakage and abrasion. Ballast degradation leads to poor drainage, rapid and excessive settlement and reduced lateral stability, which adversely affect railroad track performance. Further, high levels of degradation in ballast may cause service interruptions and safety concerns. Aggregate breakdown and crushing is the source of nearly 76% of the ballast degradation encountered in the field [1]. Maintenance of an existing track for serviceability depends on periodic inspections to assess ballast condition in terms of severity and trends of degradation with accumulated freight tonnage. Excessive ballast degradation levels combined with high moisture contents may potentially lead to decreases in shear strength properties, leading to ballast differential settlement and alteration of the track geometry [2, 3, 4].

Two indices are commonly used in the North American railroad system to quantify ballast degradation conditions. These are Selig's (i) Fouling Index (FI) and (ii) Percentage Fouling [1]. FI is the summation of percentage by weight of dry ballast material passing the No. 4 (4.75 mm) sieve and the percentage passing the No. 200 (0.075 mm) sieve. Percentage Fouling is the ratio of the dry weight of material passing the 3/8 in. (9.75 mm) sieve to the dry weight of the total sample. To estimate the amounts of larger aggregate particles vs. fine materials, traditional methods for degradation assessment involve on-site visual inspection by experts, and ballast sampling and testing through sieve analyses in the laboratory. The locations along the track where ballast samples are obtained can introduce extreme variability in the reported FI values. Like any other sampling method, ballast sampling may miss the worst field conditions. Furthermore, visual inspections by experts are also highly dependent on the level of track inspector's experience and hence can be subjective. Therefore, for a more reliable evaluation of the proper functioning of existing ballast layer, and thus the need for serviceability, it is necessary that the degradation of ballast be objectively monitored in a consistent, efficient, and preferably automated fashion. This would ensure properly quantifying fouling and overall field degradation trends of ballast throughout its service life. In view of recent advances in the area of computer vision, machine vision based inspection systems trained on example images have the potential for directly assessing ballast condition and degradation trends from images of ballast cross sections. Image segmentation has been implemented to study the individual ballast particles collected in the field in terms of their shape and size variability versus depth of sampling [5, 6]. Development and validation of a new system for on-site evaluation and quantification of ballast degradation trends and fouling conditions using non-contact sensing via machine vision is the subject of this IDEA research to adequately address the non-class specific defects and improve the Nation's rail network safety.

3.1. LABORATORY BALLAST IMAGING EXPERIMENTATION

To reproduce ballast cross sections at different degradation levels in the laboratory, samples of five different ballast materials were collected from in-service track. This was part of a recent field study that investigated in-track performance trends of different ballast materials under 36-ton axle load coal trains undertaken by Union Pacific (UP) Railroad and the Transportation Technology Center, Inc. (TTCI), sponsored by the Association of American Railroads (AAR) and the University of Illinois at Urbana-Champaign (UIUC) [7]. The samples were collected from UP Railroad's South Morrill subdivision near Ogallala, NE. The South Morrill subdivision carries approximately 230 Million Gross Tons (MGT) of coal traffic annually on Track 2, and is the location of the western Heavy Axle Load (HAL) revenue service test mega-site.

3.1.1. Sampling from In-Service Track to Collect Ballast at Different Degradation Levels

As part of Task 1 of the research project, ballast was sampled during the installation in November 2010 and additional samples were taken with a small backhoe twice a year until November 2013 at estimated traffic levels of 234, 320, 480, 538, and 732 MGTs. Rock mineralogy for each type of the ballast sources is listed in Table 1. In total, 25 samples were collected from the field at each tonnage level to generate a database for the development of the laboratory ballast imaging experiment. Each bucket of ballast was labeled with three numbers. The first number showed the ballast type, such as 1, 2, etc., the second number showed the MGT level when it was sampled, such as 234, 320, etc., and the last number referred to the sample number, e.g. 1, 2, etc. This labeling terminology is later used in this report to show sieve analysis and image processing results related to each sample.

TABLE 1. Rock Mineralogy for Ballast Types Used

Ballast Label Number	Rock Type
Type 1	Granite
Type 2	Basalt
Type 3	Quartzite
Type 4	Rhyolite
Type 5	Basalt

3.1.2. Laboratory Sieve Analysis to Achieve Ground Truth Data

A total of 25 field-collected ballast samples at different degradation levels were sieved according to the ASTM C136 standard sieve analysis procedure for coarse aggregates. The aim was to collect representative ballast samples with different FI values from clean to heavily degraded (see Figure 4). By determining the particle size distribution for each sample, ground truth data sets were generated and later was used to validate the results from the image processing algorithm. Sieve analysis was conducted using a two-stage process. First, the coarse fraction of the sample (particles with sizes above 0.5 in. (12.7 mm) was sieved using a Gilson Ts1 large aggregate screener sieve shaker. Then, the fine fraction of the ballast sample was sieved using a DS110 DuraShake rotation aggregate sifter. In total, 13 sieve sizes were used to obtain the full particle size distribution curves of the field-collected ballast samples.

From this sieve analysis, Selig's FI values were computed for the ballast samples and are reported in Appendix I and also shown in Figure 5, sorted from the lowest to highest FI values. The FI values for the 25 field collected samples varied from 0.58 to 26.9 with most of the contribution coming from passing No. 4 (4.75 mm) sieve size. Although no sample was found to have an FI value above 30, it was decided that the range of degradation values for the 25 samples was appropriate to study the performance of the proposed image processing method in estimating ballast fouling conditions. The variability of FI values at different MGT levels is due to inconsistent sampling, tamping effects, as well as dumping new ballast on the track for geometry corrections. The exact history and amount of tamping performed on individual sampling locations was unknown. Later, Section 3.1 of this report describes ballast sampling following a consistent procedure to obtain samples at higher FI values such as close to 40 and above.

Category	Fouling index (Selig and Waters 1994) (%)	Percentage of fouling (%)	Relative ballast fouling ratio (%)
Clean	<1	<2	<2
Moderately clean	1 to <10	2 to <9.5	2 to <10
Moderately fouled	10 to <20	9.5 to <17.5	10 to <20
Fouled	20 to <40	17.5 to <34	20 to <50
Highly fouled	≥40	≥34	≥50

FIGURE 4. Categories of ballast fouling defined by Selig and Water [1]

3.1.3. Recreating Ballast Cross Sections in Laboratory using Plexiglas Boxes and an Imaging Tray

A large number of laboratory ballast cross sectional images were needed to evaluate the performance and robustness of the image processing algorithm in terms of level of accuracy in identifying different degradation levels. Initially, the research team designed a Plexiglas box to reproduce vertical cross sections of ballast materials for visual investigation and image analyses at different degradation levels. The box was manufactured with dimensions of 30 in. (762 mm) width, 20 in. (508 mm) height and 9 in. (229 mm) depth out of acrylic sheets with thickness of 0.25 in. (6.35 mm). The Plexiglas box provided a good means to create clear images of vertical representations especially of new ballast cross sections in the laboratory. The images collected early on were used to start the development of the machine vision software. However, when experimenting with samples at higher degradation levels there were imaging issues; the fine dust from the field ballast samples tended to stick to the sides of the box obscuring the views of the particles inside (see Figure 6). Note that the most challenging task of any successful machine vision system is acquiring high quality images, which should show clear views

of all objects of interest for image analysis. The image of the ballast cross section shown in Figure 6 does not satisfy this requirement.

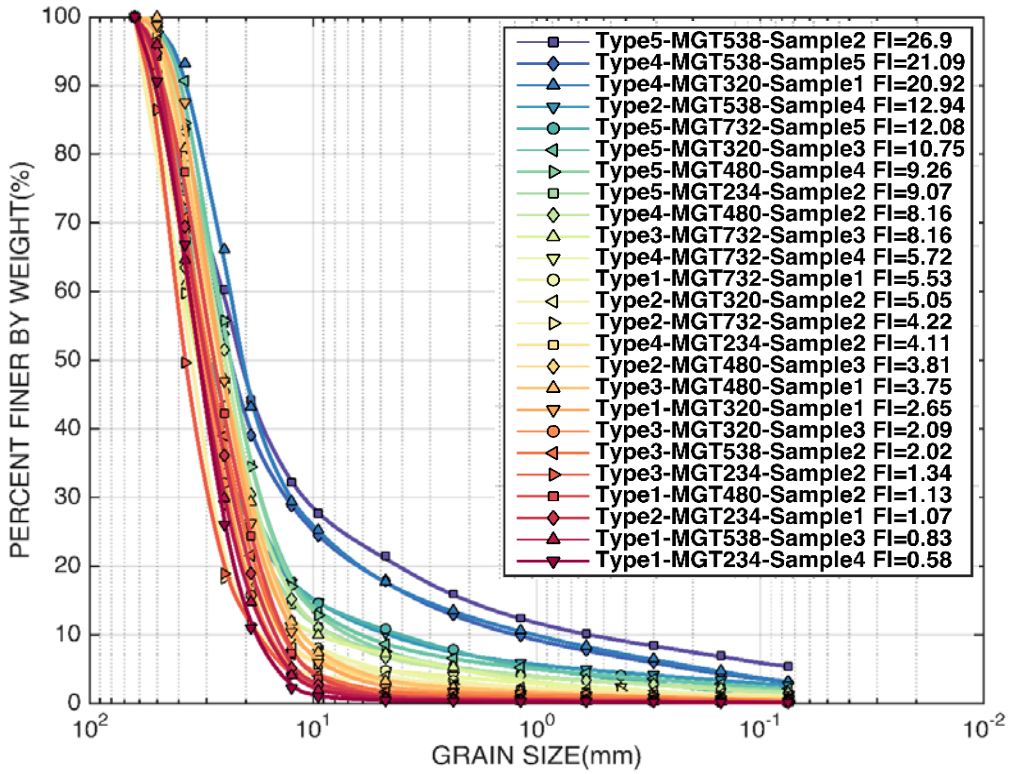

FIGURE 5. Gradation curves and corresponding Selig's FI values for 25 ballast samples at five different MGT levels collected from the UP ballast box study

FIGURE 6. Plexiglas box filled with a relatively clean field collected ballast sample at FI = 1 still causing streaks of dust from fines on the Plexiglas walls

As a second attempt to reproduce vertical cross sections of field collected ballast samples in the laboratory, a 24 in. (609 mm) wide by 21 in. (533 mm) height and 24 in. (609 mm) deep metal box with sliding doors in the front and the back was manufactured. Please see Figure 7 for the illustration of the conceptual design and the manufactured components. A sheet of clear non-scratch Plexiglas (0.5 in. (12.8 mm) thick) was positioned in the front face of the box to get a visual of the ballast depth profile. The design consisted of using two steel doors on one side of the box with the interior steel door used during sample placement and an additional external metal sliding door to protect the Plexiglas from shattering in case of

excessive ballast pressure. Note that both the external and internal sliding metal doors were lifted during capture of the image of the ballast cross section. One advantage of this metal box compared to the previously described Plexiglas setup was that it could be filled and emptied much quicker with minimal scratching of the glass. Several trials were made to reproduce vertical cross sections of ballast. Nevertheless, it was finally concluded that the reproduced cross section images of the ballast samples using the newly designed metal box did not produce satisfactory results. Please refer to Appendix II for further details related to experimentation as well as captured images with the metal box.

Finally, a tray-based design was developed for capturing top views of ballast samples using a camera placed above the tray (see Figure 8). The design enables easy loading of ballast samples onto the tray. Additionally, unloading was done by a rolling and tilling method to pour the contents for the tray back into the bucket. The detail process of capturing the top views of ballast cross section can be found in Appendix II. This process could be rapidly repeated as in a production-like setting. This provided different cross-sectional views of the same ballast sample to generate additional images for constructing an image database for use in developing our image processing algorithms.

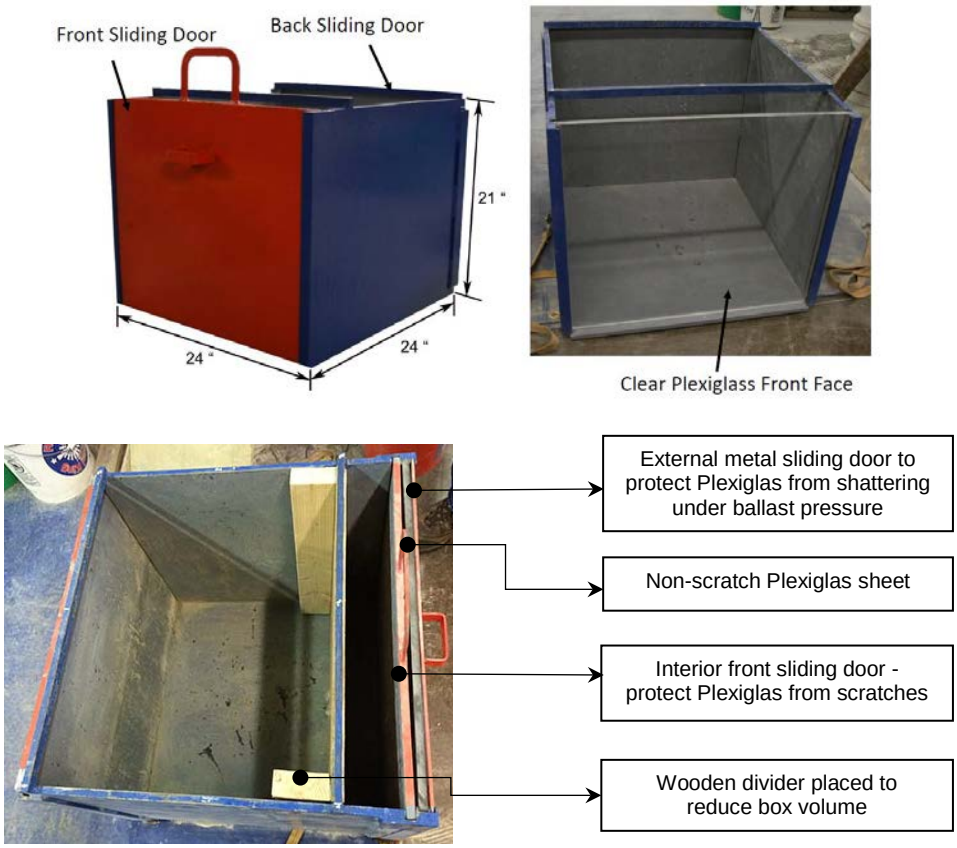

FIGURE 7. New metal box with the wooden divider and front facing clear Plexiglas

Our early work incorporating the Plexiglas box was instrumental in the development of image analysis and segmentation algorithm particularly for processing images of clean ballast samples. However, the dust generated from ballast samples with higher levels of degradation made it difficult to use the Plexiglas or even clear non-scratch glass based laboratory setups. Therefore, the ballast imaging tray method described was established as an effective and expedited laboratory imaging process to produce a large enough database of images. Each ballast material was placed on the imaging tray and photographed five times in different trials. The top view images of all 25 ballast samples at different trials and MGT levels are included in Appendix II of this report. Note that reproducing realistic images of the field-collected ballast cross sections is difficult in a laboratory environment. Therefore, there is a need for obtaining large quantities of field images by other means, such as using a field imaging kit or ideally mobile platforms such as SBCs, which is the approach that will be further described in this report. Section 3.1.4 presents essential formal testing of image analysis and segmentation algorithms under realistic field conditions.

FIGURE 8. Foreground: Ballast Imaging Tray System, Background: Bucket samples and Plexiglas box (left) - Pouring bucket containing ballast sample into the imaging tray (right)

3.1.4. Ballast Image Processing Methodology to Compute Percent Degraded Segments

The flow chart shown in Figure 9 depicts the general procedure used by the image-based inspection system. A core component of this algorithm is a three-stage image processing module, which includes pre-processing, segmentation, and post-processing. Given an image of the ballast material, such as one taken in the imaging tray, the algorithm starts with a suitable image enhancement technique, usually gamma compression, resulting in the enhanced image [8, 9]. In some cases when parts of the ballast image appear washed-out or overexposed, the histogram equalization technique [9, 10] can be used to enhance the image contrast, where most pixels in the image are concentrated in a short band of intensities. This color image is then converted to a gray scale image to apply bilateral image filtering aimed at reducing the surface texture of the ballast particles. Bilateral filtering is primarily aimed at suppressing the internal texture variations while retaining and visually enhancing the boundaries between objects [11]. Bilateral filtering is controlled by two parameters (spatial Gaussian width and range Gaussian width) [11]. The output of the preprocessing step is the input of the segmentation step, which is performed by a fine-tuned watershed segmentation algorithm.

The watershed segmentation algorithm has been shown to perform better than other leading algorithms in the presence of mutually touching particles in trench or stockpile views of ballast aggregates [12]. When individual ballast particle analysis is desired, the segments are passed through a convex hull test to filter out true and false segments. Individual ballast particles are generally expected to be convex or at least "nearly convex." This hypothesis is tested on each of the segments that are identified during the watershed segmentation step. This convexity test constructs for each segment its convex hull and computes the ratio between the area (number of pixels) of the segment and the area of the convex hull. A segment is rejected (i.e., declared not to be an actual ballast particle) if the above ratio falls below a certain adjustable threshold. A threshold value in the range of 0.6 to 0.75 has been found to be preferable (see Figure 10).

Once processed, a ballast image yields a collection of image segments that approximately capture the individual ballast particles. This output can be further utilized for many other specific analyses. For example, properties such as particle size and angularity can be assessed for each output segment, and distributions can be estimated over the entire ballast image. A visual depiction of the different image processing steps is depicted in Figure 11, which shows an example image of a top view of a ballast sample placed inside the tray.

The degradation analysis on each segmented image is conducted using an area-based approach to identify the corresponding size categories for valid ballast particles and degraded particle zones (see Figure 11). For this effort, the known area of a 1 in. (25.4 mm) diameter calibration ball, in terms of the number of pixels, is used to estimate the area of each segment. The segments are then partitioned into three size categories (typical, small and large). The typical category represents average size ballast particles, the small category represents severely degraded particles, and the large represents oversized areas with particles too small to be identified individually, such as fine-grained soils. These categories are determined by normalizing the areas with respect to the area of the calibration ball and setting thresholds at less than 60% for small and more than 300% for large. The later categories are labelled as degraded segments.

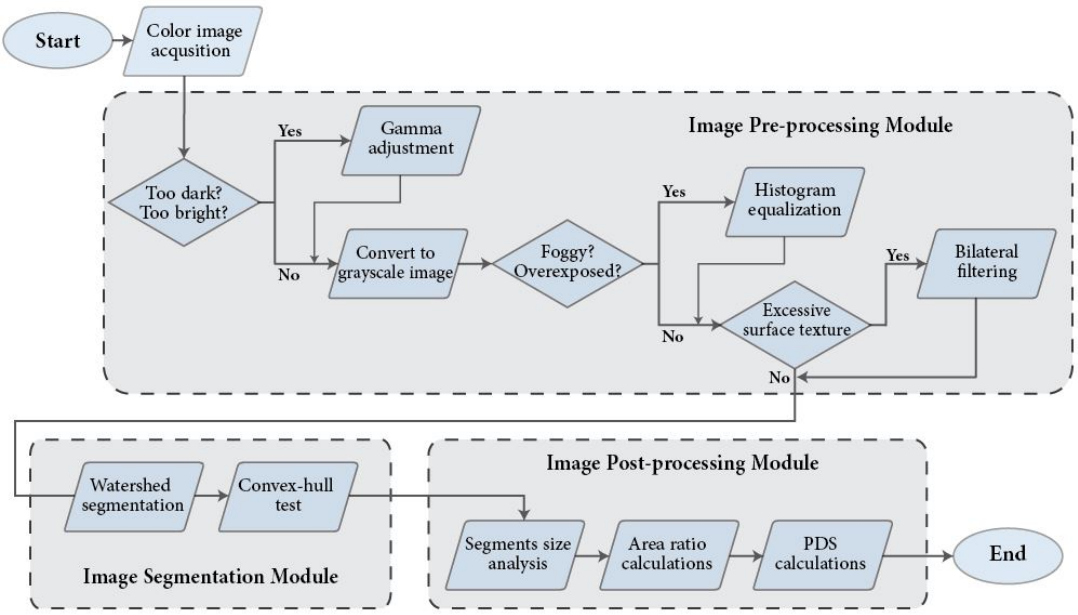

FIGURE 9. Flowchart of image analysis and segmentation algorithm

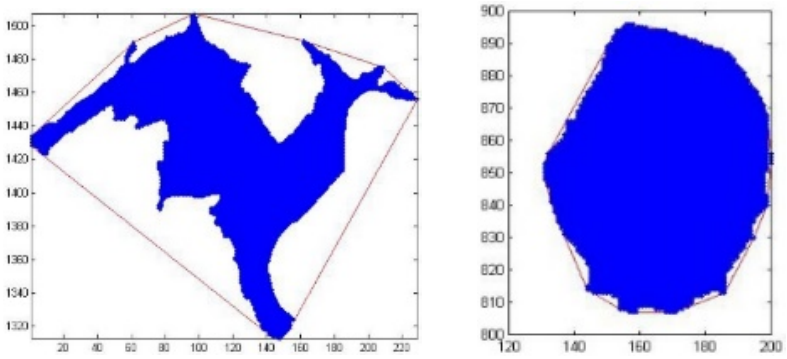

(a) (b)

FIGURE 10. (a) Convex hull (boundary) of a false-segment (non-ballast particle) and (b) Convex hull of a true-segment (ballast particle) – [Note: axes are pixel locations in the image]

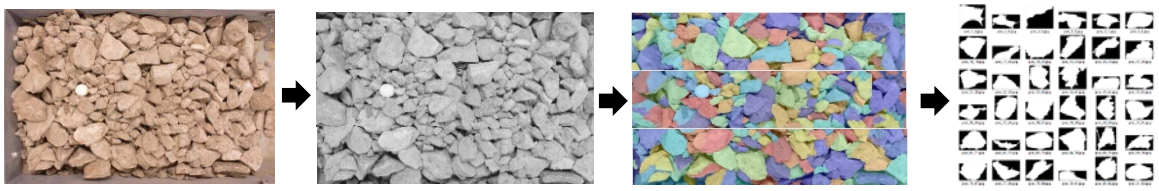

Laboratory Ballast Image Acquisition in the Tray ***Image Filtering and Enhancement*** ***Watershed Segmentation and Convex-hull test*** ***Segment Size and PDS Calculation***

FIGURE 11. The image processing steps. The example image shown here is the top view of a ballast sample placed inside a tray. A 1 in (25.4 mm) diameter white ball was placed for image calibration purposes

A score for each image, called Percentage of Degraded Segments (PDS), is defined as the percentage of the total area of large and small segments compared to the total area of the ballast image. Let S_i ($i = 1,..., n$) be the areas of the segments $1,..., n$ in the image. Let b be the area of the 1 in. (25.4 mm) diameter calibration ball and A be the area of the image. Note

that all areas are measured in terms of pixels/inch. Then, the PDS value in terms of percentage can be computed using Equation 1 as follows:

Eq. 1:

$$Define: J = \{1 \le i \le n \mid threshold_s < \frac{s_i}{b} < threshold_l,\ threshold_s = 0.6,\ threshold_l = 3\}$$

$$Then,\ PDS(\%) = 100 \times (1 - \frac{\sum i \in J\ s_i}{A})$$

Note that achieving a desirable segmentation of each ballast image, at differing degradation levels, needs iterative interaction from the user with the algorithm. This involves fine-tuning the segmentation parameters related to bilateral filtering, watershed segmentation, and convex-hull threshold criteria. A trained user can complete the processes in two to three minutes adjusting the three sets of parameters. Typically, two or three iterations are required before achieving the desirable outcome. Generally, less than an hour is needed for training and it may take a couple of hours of practice for the user to get more efficient. Using the GUIDE tool in Matlab [13], a Graphical User Interface (GUI) was developed to facilitate processing the captured images and to provide an efficient tool to adjust segmentation parameters. A screenshot of this GUI is shown in Figure 12. The main segmentation parameters and their use are described briefly in this section.

Spatial Gaussian Width and Range Gaussian Width

The bilateral filtering of an image at pixel position p relative to pixel position q with intensity I is given in Equation 2 as follows:

Eq. 2: $$BF[I_p] = \frac{1}{w_p} \sum_{q \in s} G_{\sigma_s}(\| \mathrm{p} - \mathrm{q} \|)\, G_{\sigma_r}(| I_p - I_q |)\ I_q$$

where $1/w_p$ is the normalization factor, G_{σ_s} and G_{σ_r} are the Gaussian spatial kernel and the Gaussian range kernel respectively. Equation 2 is a normalized weighted average where $G_{\sigma_s}$is a spatial Gaussian that decreases the influence of distant pixels, G_{σ_r} a range Gaussian that decreases the influence of pixels q with an intensity value different from *Ip*. Consider the pixel of interest at position *p*, the Spatial Gaussian width, represented by σ_s, determines the size (number of pixels) of the Gaussian window used to smooth images. In other words, the Spatial Gaussian width is the size of the considered pixel neighborhood (thinner than $2\sigma_s$) used to calculate the average intensity of pixel at position *p* [14]. Also, because bilateral filtering retains the boundaries of ballast particles, one needs the Range Gaussian width, denoted by σ_r, to represent the minimum amplitude of an edge, so that the pixels in the considered neighborhood whose intensity is above or below this boundary are ignored in the smoothing process. In ballast images with 3158 × 4152 pixels, σ_s and σ_r could range from 3 to 200, but since some ballast boundaries before the preprocessing stage are already blurred, it is preferable to keep σ_s below 20 and σ_r below 10.

Strel-Size 1

The strel size describes the radius (number of pixels) of a disk-shaped morphological structuring element used to clean up the ballast particles, thus enhancing the segmentation results. It is found that in ballast images captured in the laboratory with 3158 × 4152 pixels, the strel-size needs to be 12 to 16 to segment 1 in. (25.4 mm) ballast particles, 16 to 20 for 2 in. (50 mm) particles, and 20 to 30 for 3 in. (76 mm) particles.

Number of Pixels for 1-in. (25.4 mm) Ball

The number of pixels for 1 in. (25.4 mm) calibration ball indicates how many pixels are needed to represent 1in. (25.4 mm) diameter circle in the image. The user can obtain this value at the pre-processing stage using the GUI.

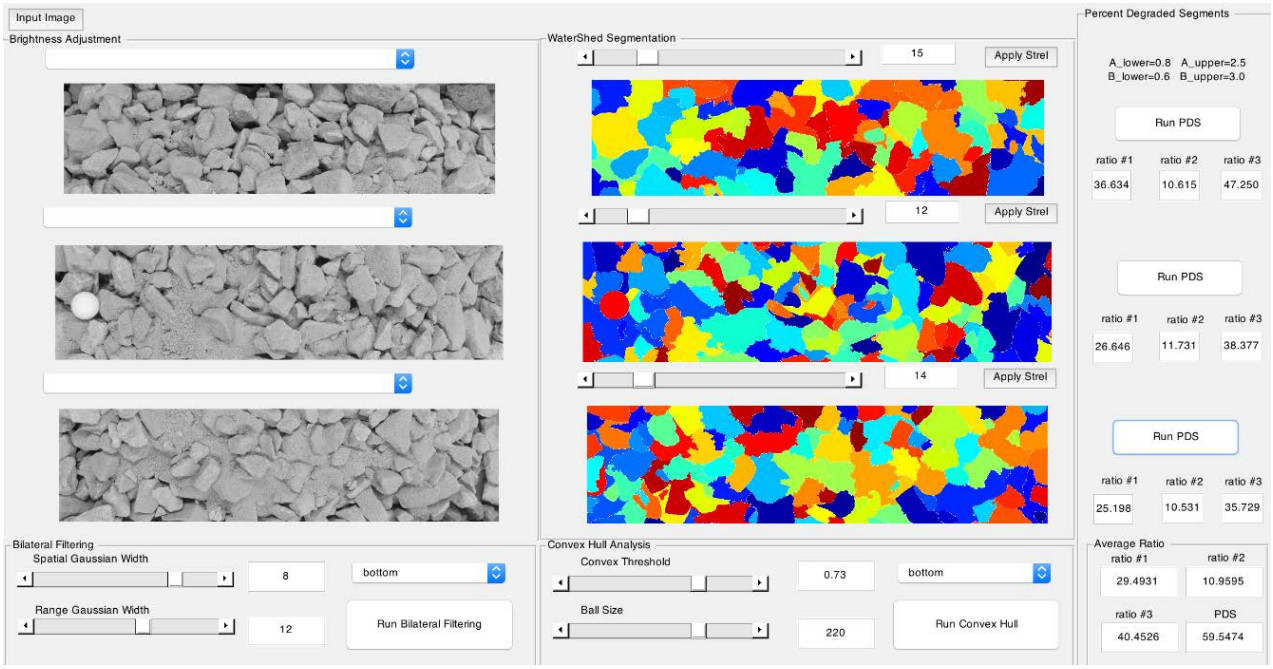

FIGURE 12. Graphical User Interface (GUI) for degradation evaluation of ballast images

Convex-hull Threshold

The convex hull of a set *X* of points in the Euclidean space is the smallest convex set that contains *X*. For instance, when *X* is a bounded subset of the plane, the convex hull may be visualized as the shape enclosed by a rubber band stretched around *X* [15]. In the developed algorithm, the convex-hull threshold falls between 0.6 and 0.75.

During the analyses of ballast images, it was observed that the performance of the segmentation algorithm in terms of precise detection of ballast particles and/or degradation zones was dependent on the level of particle size variability in each image. In other words, identifying one single set of segmentation parameters capable of detecting both small and large ballast particles for the entire image area was found to be very challenging. Consequently, it was decided that each ballast image would initially be cropped into three identical sub-images representing the upper, middle and lower portions of the captured ballast cross section (see Figure 12). The reason for creating three sub-images is to better capture the expected increase of ballast degradation that corresponds to the increase in ballast layer depth, as observed previously for in-service track [5]. Therefore, the variability of particle sizes processed in each sub-image is expected to be less than the variability of particle sizes of the entire image. Through visual observation of the segmentation results, this approach proved to increase the performance of the algorithm. Thus, three sets of segmentation parameters and PDS values were recorded for each ballast image. Therefore, the final PDS value for each image was reported as the average of the three PDS values associated with three sub-images.

3.1.5. Image Processing Results and Discussion on Variability of PDS versus Severity of Ballast Degradation

The image processing methodology described in the previous section was applied to all the 125 top view images of the field-collected ballast samples inside the tray. For each image, the average PDS was computed and compared with the associated Selig's FI value obtained through sieve analysis for the corresponding sample. As an example, Table 2 presents a typical image segmentation result for three representative images collected at low, medium, and high degradation levels.

The PDS values for the 125 images and the size in pixels of 1 in. (25.4 mm) calibration ball used in the analyses are listed in Appendix III of this report. From the field samples, the means of the average PDS values from five trials typically range from 45% to 68% and the standard deviations vary from 0.866 to 7.33. The PDS values are reported with the accuracy of two decimal points similar to FI.

TABLE 2. Sample Image Segmentation Results for Ballast Placed Inside a Tray with Low, Medium, and High Degradation Levels, whose Top View Images Are Shown Left to Right

Selig's Fouling Index = 2.09	**Selig's Fouling Index = 12.94**	**Selig's Fouling Index = 26.90**
		
Image ID: 3-230-3 at trial 4	*Image ID: 2-538-4 at trial 2*	*Image ID: 5-538-2 at trial 4*
	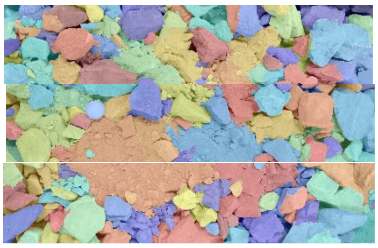	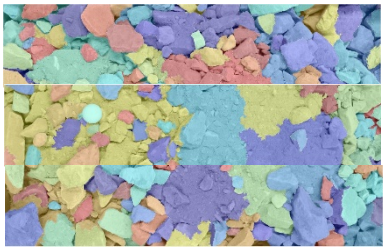
Average Percent Degraded Segments = 56.37 %	**Average Percent Degraded Segments = 64.03 %**	**Average Percent Degraded Segments = 69 %**

A preliminary correlation was found to exist between the Selig's FI values obtained using sieve analysis and the means of the average PDS values resulting from segmentation analyses. The linear correlation established, based on regression analysis, is presented in Figure 13. Note that this relationship was later improved by performing correlation analysis on the image processing results obtained by processing field-captured cross section images (see Figures 19 and 26). To further investigate the variability of segmentation results due to the five imaging trials in the laboratory, a linear regression analysis was performed between the standard deviation of average PDS values for five imaging trials and the FI ground truth results, as shown in Figure 14.

Note that the linear regression results presented in Figures 13 and 14 are only valid within the ranges of the FI and average PDS values that were obtained as part of this research. Nevertheless, both figures indicate that by increasing Selig's FI, the means of average PDS values as well as the associated standard deviations for five imaging trials increase. The increasing trend of the standard deviations versus FI values could be explained by the higher percentages of fine particles (passing the No. 4 sieve) found in samples at higher levels of degradation. For each imaging trial, these fine particles accumulated at different layers (depths) of the tray. Therefore, the top view of the same ballast sample placed inside the tray several times could easily appear different for each imaging trial (see Appendix II). This could have caused higher variability in the image segmentation results particularly for the samples with higher FI values.

3.2. FIELD BALLAST IMAGING OF TRANSVERSE TRENCHES IN TTCI TEST TRACK

The performance of the imaging based approach was validated using images of in-service ballast cross sections captured in the field. Additionally, ground truth values obtained from mechanical sieve analyses on 14 ballast samples collected at different degradation levels at TTCI's Facility for Accelerated Service Testing (FAST) located in Pueblo, Colorado.

3.2.1. Field Imaging to Acquire Vertical Cross Sections and Collecting Corresponding Ballast Samples

To establish a database of ballast cross sections at different degradation levels, 14 ballast samples were collected. These 14 samples were captured from inside trenches that were dug perpendicular to the track at five different zones in Section three of High Tonnage Loop (HTL) at TTC. Note that before shaving off the ballast sample, a field image of each corresponding ballast cross section was captured, the sample was then taken of the particles that were directly in the field-of-view of the camera. Therefore, 14 field images, i.e., views of the ballast cut section, corresponding to 14 ballast samples were captured

and used in this study. The locations of the zones and types of concrete ties/under tie pads used in each zone are shown in Figure 15.

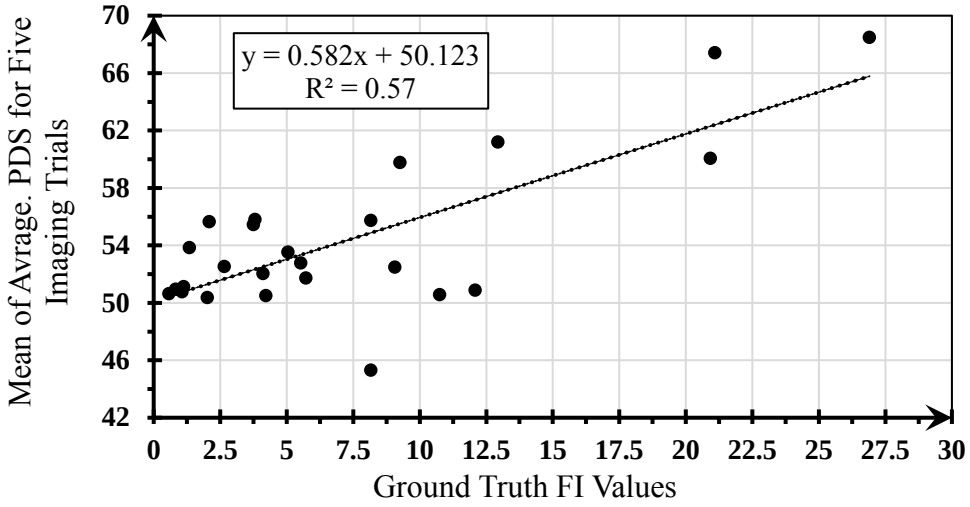

FIGURE 13. Relationship between Selig's FI values obtained from sieve analysis and the means of average PDS values for five imaging trials through ballast image segmentation

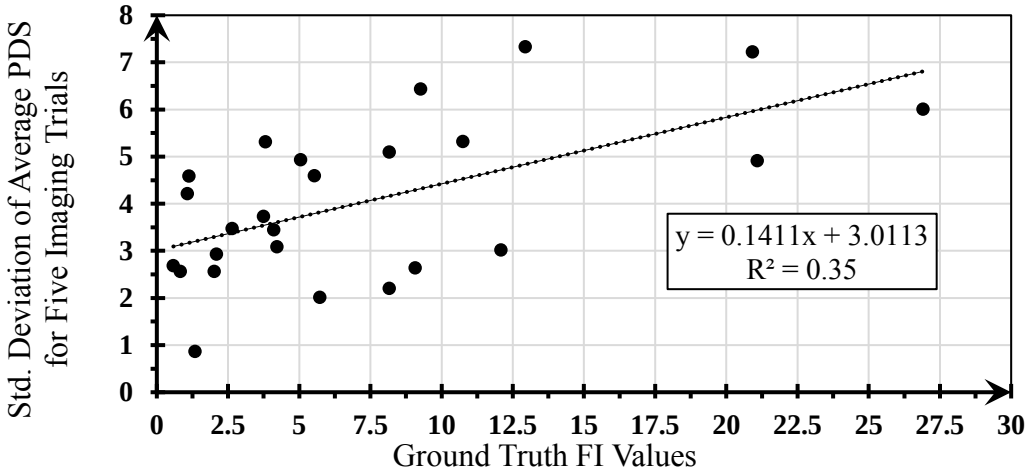

FIGURE 14. Linkage between Selig's FI values obtained from sieve analysis and the standard deviations of average PDS for five imaging trials through ballast image segmentation

The field image acquisition and sampling process included removing one tie, digging a trench with a backhoe and manually preparing a vertical face on the trench wall. The entire process is illustrated through the photos shown in Figure 16. Further description related to image acquisition and sampling can be found in Appendix IV.

A consistent spatial resolution, i.e. number of pixels used per unit length, was maintained across the entire image. To provide this, the optical axis of the camera lens was made normal to the cross section and the setting for the camera aperture was adjusted to provide the least lens distortion. In addition, the camera zoom was adjusted so the field of view covered the same surface area, 24 in. (609 m) × 16 in. (406 mm), in each image (providing approximately 80 pixels/cm). This ratio was verified by determining the number of pixels covering a 1 in. (25.4 mm) diameter spherical calibration ball placed in the ballast image view. This step was essential to determine the exact particle measurements in each image (see Step 3 in

Figure 16). These steps ensured the uniformity of the output data from the machine vision algorithm, by making appropriate adjustments based on any slight difference in size of the calibration ball measured in the image.

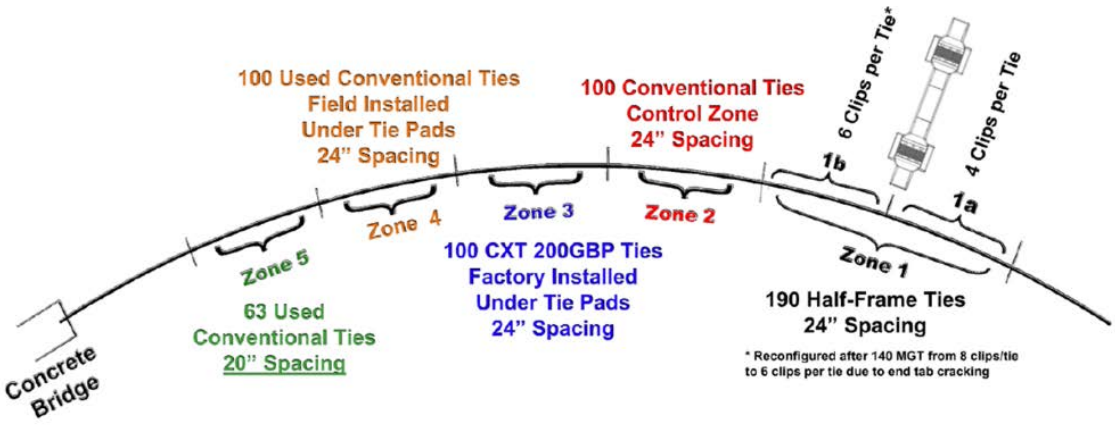

FIGURE 15. Zone locations and types of concrete crosstie and under tie pads in HTL Section 3 – TTCI

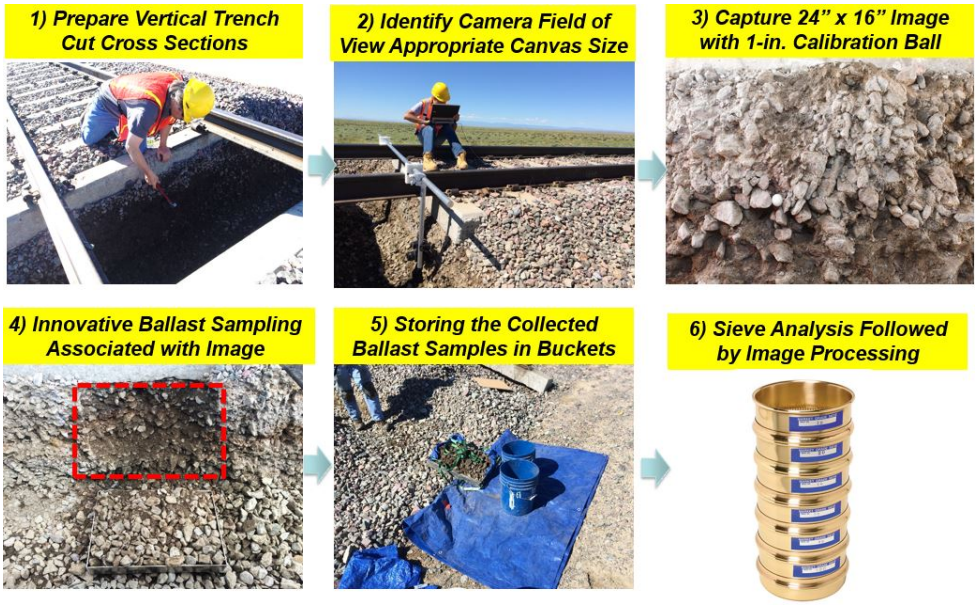

FIGURE 16. The procedure for trenching, imaging and novel ballast sampling in HTL Section 3 – TTCI

3.2.2. Laboratory Sieve Analysis to Achieve Ground Truth Data

Fourteen field-collected ballast samples at different degradation levels were sieved according to ASTM C136 specification with the sieve analysis procedure/equipment described earlier in this report. The full gradation curves of these 14 ballast samples are presented in Figure 17 where they are sorted from the lowest to the highest FI values. The cross-section images associated with these 14 samples are presented in Appendix IV.

Each bucket of ballast was labeled with three numbers. The first number shows zone number, e.g. 1, 2, etc., the second number shows the tie number or the location of the lateral trench, e.g. 1050, 1308, etc., and the last number refers to the imaging location inside the trench where the field image was captured, e.g. C1 (center), I1 (inside rail), etc.

Using the sieve analysis results, Selig's FI values were computed for each ballast sample. According to Figure 17, the amount of particles passing the No. 200 (0.075 mm) sieve was limited to less than 5% for all the samples. These FI values were paired with their associated ballast cross section images captured in the field.

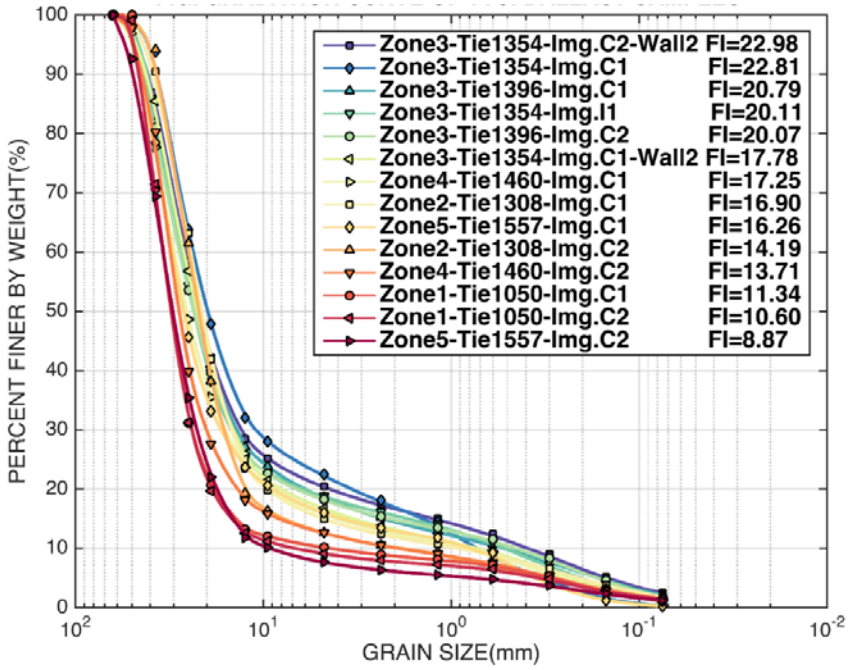

FIGURE 17. Gradation curves and corresponding Selig's Fouling Indices (FI) for 14 ballast samples collected from HTL Section 3 – TTCI

3.2.3. Image Processing Results and Discussion on Relationship between FI and PDS

The image processing methodology described previously was used to analyze the 14 images of ballast cross sections captured in TTCI HTL. The following items were encountered while performing image segmentation on the field ballast images:

(1) Tray images captured in the laboratory usually had cleaner ballast samples than observed from the field ballast images, and that the same ballast cross section might not appear the same in different tray images. Thus, the algorithm would provide less accurate analyses for laboratory images compared to field images.

(2) As mentioned in Section 3.1.4, at the post-processing stage, each segmented image is categorized as small, typical or large, and the two thresholds for these three classes are 60% and 300%. It was found that ballast particles are usually larger in tray images, and some of the segments that were expected to be "typical" fell into the large category. This problem can be addressed by readjusting the threshold values.

For each field image, the average PDS value was computed and compared with the associated Selig's FI value obtained from the sieve analysis. As an example, Figure 18 shows typical image segmentation results for three representative field collected ballast images at low, medium, and high degradation levels. Note that from the sieve analysis results (see Figure 17), the Selig's FI values were determined to be in the range of 8 to 23.

Referring to Figure 17, the percentage of materials passing the No. 4 (4.75 mm) sieve contributes more significantly to the computed FI value when compared to those percentages passing the No. 200 (0.075 mm) sieve. This indicates that degradation from particle breakage and abrasion in the field did not accumulate a considerable amount of materials passing the No. 200 (0.075 mm) sieve sized fine particles. It is important to note that this finding is only valid for the 14 ballast samples collected as part of this study and should not be generalized for any ballast sample collected from in-service railroad track.

The average PDS values and pixel size of 1 in. (25.4 mm) calibration balls are listed in Table 3. The PDS value varies from 50% to 70%, with an accuracy of two decimal points. Unlike Selig's FI, the PDS value is a function of segmentation parameters adjusted by the user. In other words, two users may produce two different sets of segmentation parameters which may lead to two differing PDS values for the same image. Note that PDS can be computed for any desirable portion of an image.

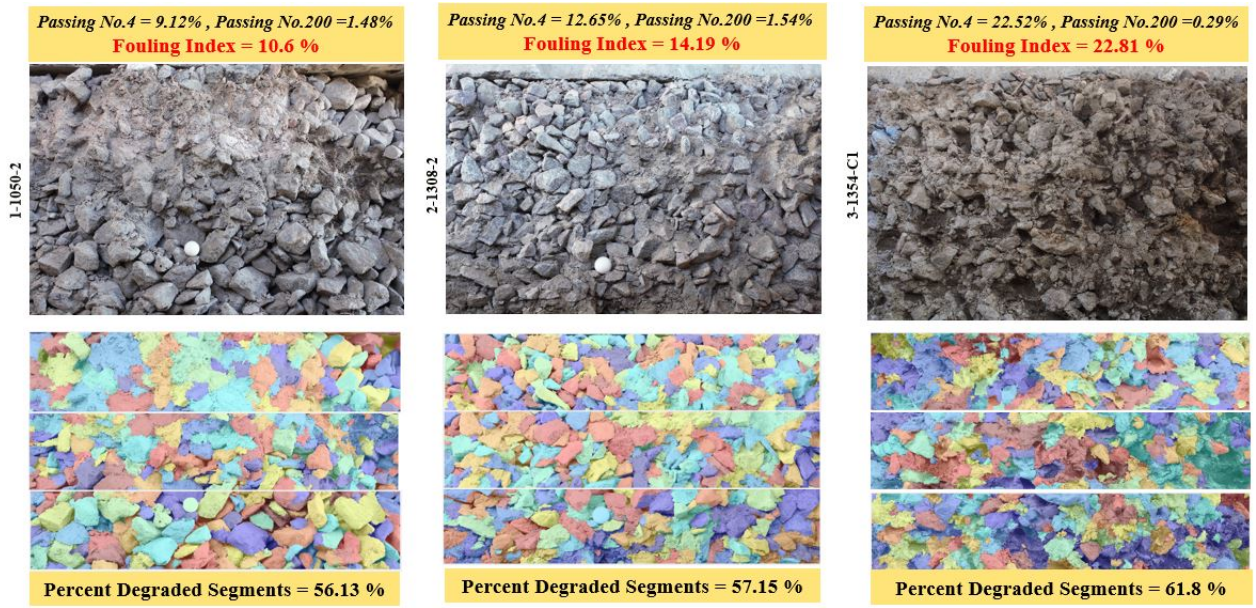

FIGURE 18. Representative image segmentation results for three TTCI HTL ballast images indicating low, medium, and high degradation levels from left to right

TABLE 3. Segmentation Parameters and PDS Values for Ballast Samples Collected in TTCI HTL

No.	Ballast sample/image ID designation	Size of 1-inch calibration ball considered in the analysis (pixels)	Average Percent Degraded Segments (PDS) (%)
1	1-1050-C1	202	50.94
2	1-1050-C2	196	50.14
3	2-1308-C1	221	57.82
4	2-1308-C2	221	53.82
5	3-1396-C1	231	55.25
6	3-1396-C2	216	62.53
7	4-1460-C1	186	58.05
8	4-1460-C2	192	52.98
9	5-1557-C1	192	61.21
10	5-1557-C2	169	50.31
11	3-1354-I1	195	61.28
12	3-1354-C1	196	61.80
13	3-1354-C1-Wall2	157	59.01
14	3-1354-C2-Wall2	145	70.04

A correlation was established between the Selig's FI values obtained from the sieve analyses of the collected ballast samples and the average PDS values resulted from segmentation analyses of the TTCI HTL images. Figure 19 presents this correlation as a linear regression equation. A coefficient of determination (R-squared) value of 0.75 obtained for the linear

regression equation shown in Figure 19 demonstrates that a significant correlation existed between Selig's FI and average PDS values. Note that the linear equation shown in Figure 19 is only valid for the range of the FI and the average PDS values that were obtained as part of this study. Since Selig's FI value typically varies from 0 to 40 to represent clean to heavily degraded in-service ballast samples, respectively, more field samples and images are needed to fully develop the relationship between the FI and average PDS values.

The average values of a minimum three PDS segmentation results were computed and reported for three sub-images of each ballast image. Pairing the average PDS values listed in Table 3 with the actual ballast field images showed that average PDS could successfully make a distinction between two field ballast cross section images with low and high levels of degradations.

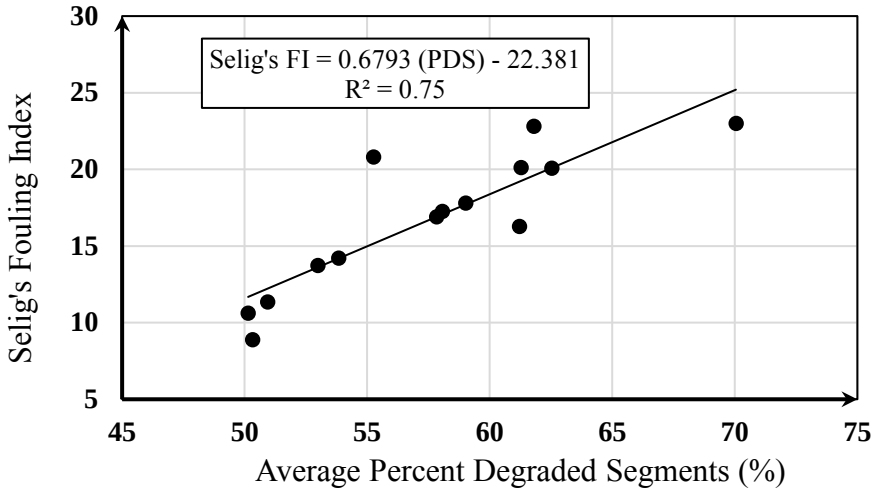

FIGURE 19. Linkage between Selig's FI values obtained from sieve analysis and PDS values obtained through ballast image segmentation on TTCI HTL ballast field images

3.3. BALLAST IMAGING THROUGH LONGITUDINAL SHOULDER CUTS ON REVENUE TRACK

An SBC provides a continuous cut section of the shoulder as it progresses down the track during track maintenance activities. Therefore, our ballast inspection system can be directly applied to quantify degradation levels, using periodically acquired images. This will provide a method for continuous evaluation of ballast degradation levels, and serve as a candidate for future incorporation of the developed technology into the SBC equipment operation. As part of the Stage 2 scope of this research project, shoulder ballast field imaging and sampling on revenue track was further investigated to evaluate the performance of our algorithm.

3.3.1. Field Imaging at Active Shoulder Ballast Cleaning Site with SBC Equipment

A field imaging trip was arranged in coordination with Loram Maintenance of Way to visit an active shoulder ballast cleaning site on Union Pacific Track near Marlinton, IL. This was part of an effort to capture horizontal ballast cross section images generated by SBC equipment. Ballast cleaners use 30 in. (762 mm) wide digging buckets to dig and scoop ballast from the tie ends outward to the edge of the ballast section while scarifier teeth undercut the tie ends to 5 in. (127 mm). A conveyor transfers the fouled ballast to a series of vibrating screens where fines are separated and discharged. SBC equipment then distributes the cleaned ballast along the shoulder and regulates the returned ballast to the shape specified by the railroad. Based on the previous experience of the research team, it was expected that there would be a sufficient time window available between the digging wheel and clean ballast hopper door which would allow to capture the images of the exposed shoulder cross section. However, upon arrival to the site it was found that this particular model of SBC (SBC-15) had a short distance between the digging wheel and clean ballast hopper door. This would not provide enough space to capture the image of the exposed shoulder cross section. Note that this was an older SBC and most shoulder cleaning equipment would not have this constraint. After discussing with Loram personnel, it was agreed to follow a modified procedure as described below to capture shoulder images and ballast samples to overcome this challenge.

Once the SBC equipment was ready to move down the track, the imaging crew was positioned at a location in front, marked a designated area for sampling, and dug down to depth of 6 in. (152 mm) below the tie in the shoulder using pick-axe and spade. A horizontal cross section was prepared, images of 24 in. (609 mm) by 16 in. (406 mm) canvas size were captured and samples were collected at two locations. Then, the SBC equipment was allowed to approach, pass the pre-sampled area at normal speed while the clean ballast hopper door closed. This would provide a second exposed cross section of the shoulder generated by digging wheel at approximately the same depth of 6 in. (152 mm) below the tie. Then, the SBC equipment stopped to allow the imaging crew to capture the second horizontal shoulder cross section image of the same area. Following the image acquisition stage, the SBC equipment reversed back to the imaged location to dump the clean ballast and cover the exposed cross section. The imaging and sampling stages are further described in Figure 20. Note that no sample was taken from the shoulder cross section after SBC pass.

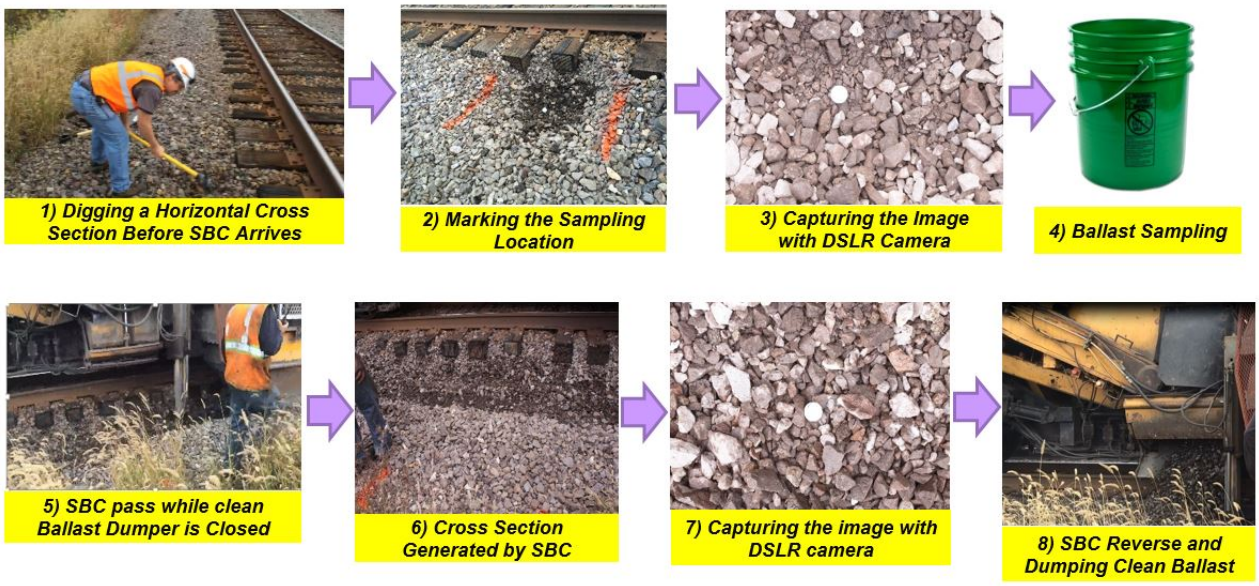

FIGURE 20. Shoulder ballast image acquisition procedure with SBC equipment

Note that due to limited track access, there was not enough time to re-take additional ballast samples after capturing the second image, but the first sample was treated as representative of the marked area. Two locations were investigated before the shoulder cleaning activity was terminated by the track owner because of heavy train traffic. After discussing with SBC manufacturer, it was found that most of current and future generations of SBCs have a considerable distance between the digging wheels and the clean ballast hopper. However, due to project time limitations the research team developed an alternative method for collecting additional horizontal shoulder cross section images similar to those generated by an SBC. This process will be further discussed in the next section.

Figure 21 shows the gradation curves for the samples collected from locations one and two. This figure shows that the two sampled locations possessed relatively low degradation levels indicated by FI values of 1.96 and 9.00. The captured images of shoulder cross sections before and after the SBC pass for locations one and two are also shown in Table 4. These images were processed using the ballast image processing algorithm to obtain associated PDS values. As shown in Table 4, the PDS values corresponding to before and after the SBC pass at a certain location are very similar. This finding confirms that the initial horizontal shoulder cross sections generated by excavation tools and those later generated at the similar depth but with the SBC digging wheel are approximately identical in terms of the level of degradation. This finding was later considered as the basis for the development of the manual shoulder ballast imaging procedure, which will be described in more detail in the next section.

For better visual evaluation of the segmentation results, a new color-based size coding key was added to the image segmentation module. As described in Section 3.1.4, the segments are partitioned into three categories (typical, small and large), and the thresholds are set at 0.6 and 3 times the area of a 1in. (25.4 mm) calibration ball. As shown in Figure 22, small segments (less than 0.6 in.) are shown in shades of green and large segments (larger than 3 in.) are shown in shades of blue. The segments that fall into the typical category are labeled using a warm color transition from yellow to red to brown. Finally, the segments or degraded zones that did not pass the convex-hull test are labeled purple (indicated in Figure

22 as degraded zones). This new color size coding key is helpful for interpreting the results and also for assisting users to fine-tune the watershed segmentation parameters.

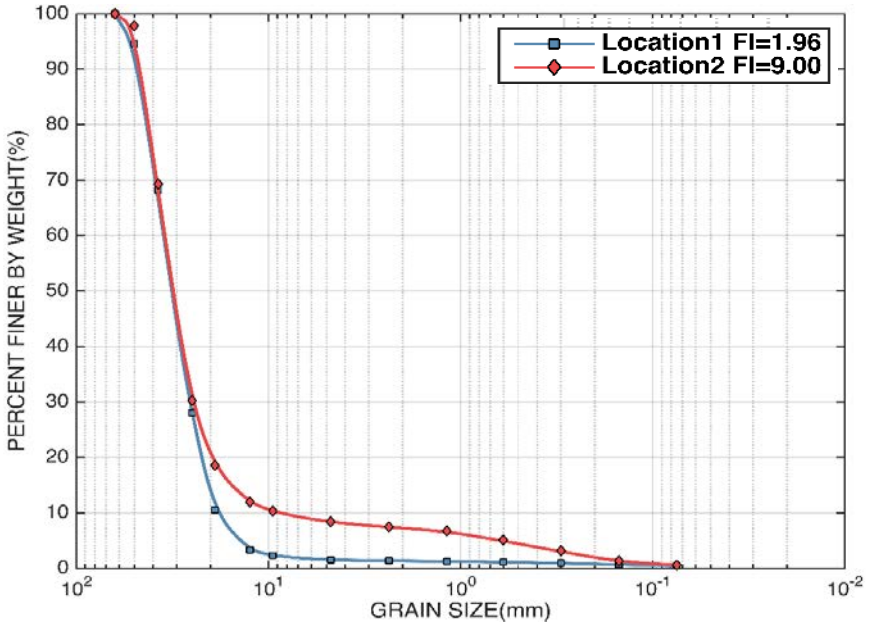

FIGURE 21. Gradation curves for the two samples collected ahead of the SBC from locations one and two

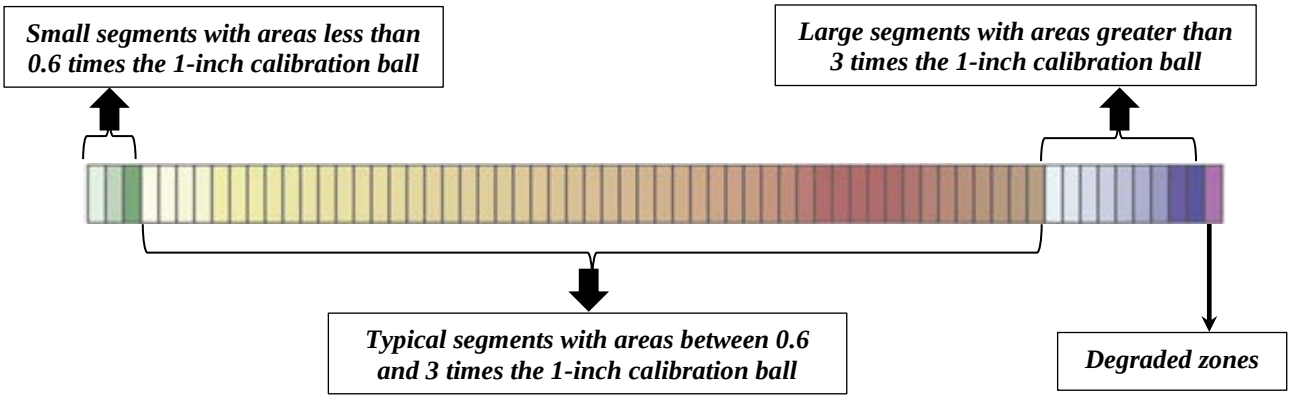

FIGURE 22. Color coded key to represent ballast image processing results considering sizes of segments

3.3.2. Manual Shoulder Ballast Imaging to Emulate Horizontal Cross Sections from SBC

A field imaging trip was arranged with the help and support of BNSF Railway to visit several track locations near Kansas City, MO with the intent to collect images and samples of horizontal ballast shoulder cut sections at different degradation levels. This was part of evaluating the capability and reliability of the imaging based ballast inspection system to assess degradation levels from shoulder cross section images similar to those made by SBCs. Twelve ballast samples and associated images were collected following a sampling and imaging procedure. Visual descriptions of the stages of shoulder ballast imaging and sampling are illustrated in Figure 23. Further details related to image acquisition and sampling can be found in Appendix V.

TABLE 4. Shoulder Cross Section Original and Segmented Images with PDS Values Before and After SBC Pass*

		Location One	Location Two
		Image ID: 145 FI =1.96	*Image ID: 151 FI =9.00*
Before SBC Pass	**Original Image**		
	Segmented Image	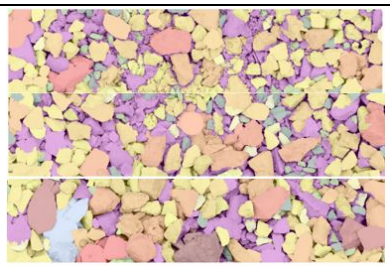	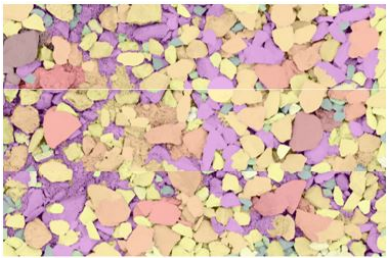
	PDS (%)	*35.94*	*34.87*
		Image ID: 163	*Image ID:184*
After SBC Pass*	**Original Image**		
	Segmented Image	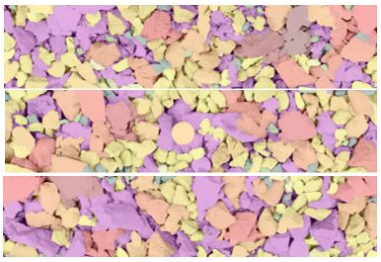	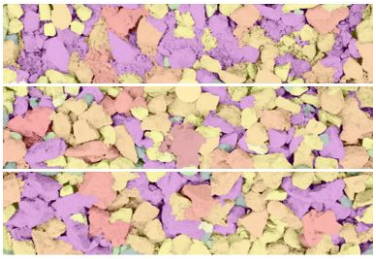
	PDS (%)	*35.4*	*35.99*

**Note: FI values are not available for After SBC Pass because samples were not taken*

Laboratory sieve analysis was performed following the same procedure that was described previously. The gradation curves for all 12 samples and their corresponding FI values are presented in Figure 24. According to Figure 24, FI values for all 12 samples varied from 4.75 to 46.04, which covers a wide range of ballast conditions from clean to heavily fouled. Note that the gradation curve representing sample at FI = 27.73 shows a drastically higher percentage of passing No. 200 (0.075 mm) sieve compared with the other samples. This is related to the special washed sieving procedure that was used for this specific sample. Due to the presence of high plasticity fine material, it was decided that dry sieving would not be an appropriate method for this sample so washed sieve analysis following ASTM C117 was conducted in the laboratory.

The image processing approach described previously was used to analyze the horizontal cross section images captured on BNSF lines near Kansas City, MO. The average PDS values and pixel size of the 1 in. (25.4 mm) calibration ball considered

in the analyses are listed in Table 5. According to this table, the computed PDS values have a large variation ranging from 35% to 81%. Note that the PDS values are reported with the accuracy of two decimal points similar to FI values.

Using the PDS values listed in Table 5, it was decided to run a validation analysis on the regression model developed in Section 3.2.3 of this report. Since the 12 samples of collected ballast for the data points listed in Table 5 were never used in regression analysis described in Section 3.2.3, it makes them a good candidate as a testing dataset to evaluate the accuracy of the model. Figure 25 shows the results of this validation analysis. According to this figure, for most of the samples at higher degradation levels, the regression model somewhat underestimated the FI values. This finding was expected because the range of FI values in the 12 testing data points is beyond the range of 14 data points that were originally used in Section 3.2.3 model. Nevertheless, the Section 3.2.3 model still showed a satisfactory performance in predicting close results from the PDS equation considering its achieved coefficient of determination as $R^2 = 0.75$. As discussed previously, the accuracy of the regression model can always be improved by expanding both quantity and range of data points in the analysis. The cross-section images associated with these 12 samples are presented in Appendix V.

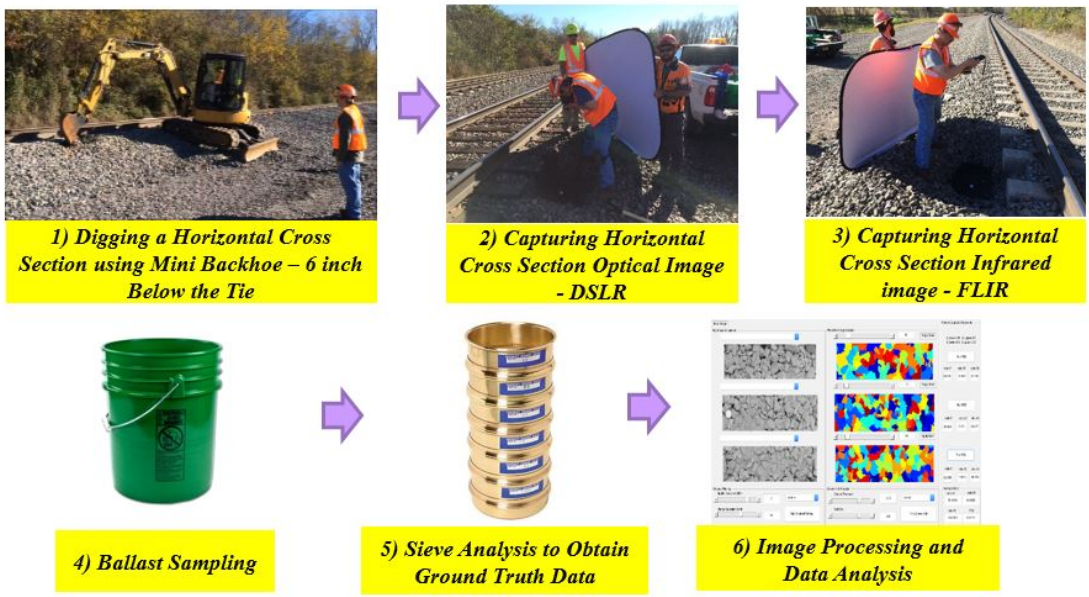

FIGURE 23. Different stages for shoulder ballast sampling and image acquisition without SBC equipment

TABLE 5. Segmentation Parameters and PDS Values for Shoulder Section Images from BNSF Track near Kansas City

No.	Ballast sample/image ID designation	Size of 1-inch calibration ball considered in the analysis (pixels)	Average Percent Degraded Segments (PDS) (%)
1	75-76-77	300	35.24
2	07-08-09	276	49.8
3	39-40-41	208	34.87
4	78-79-80	300	42.64
5	87-88-89	285	50.68
6	50-51-52	300	74.62
7	34-35-36	226	68.39
8	47-48-49	288	59.12
9	38-39-40	246	68.39
10	81-82-83	300	74.11
11	63-64-65	300	87.09
12	20-21-22	294	81.19

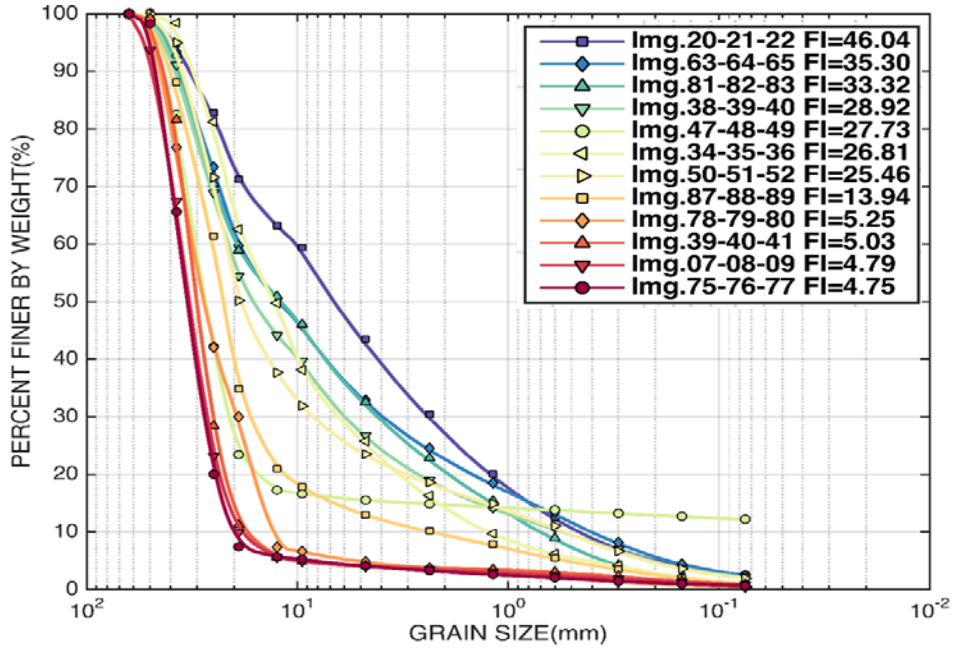

FIGURE 24. Gradation curves for 12 samples collected from shoulder sections on BNSF track near Kansas City

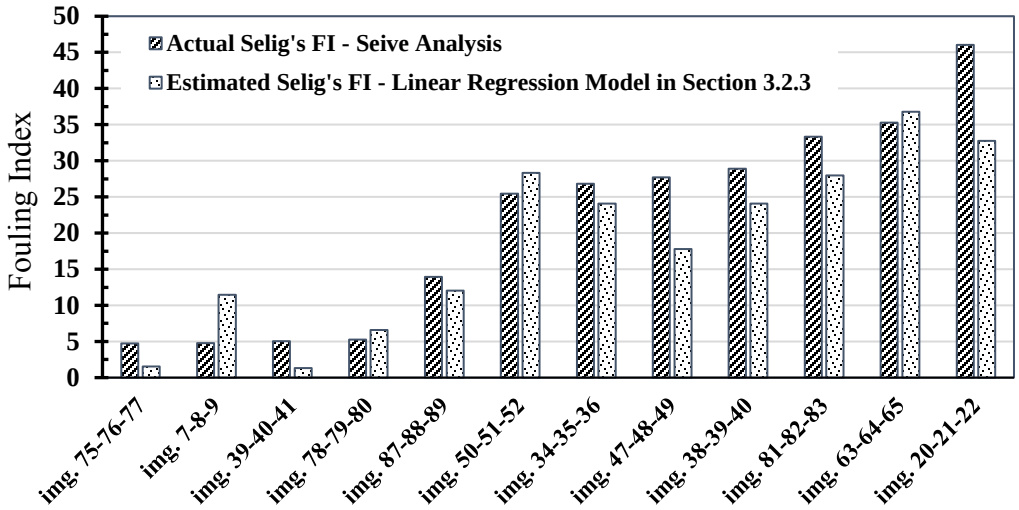

FIGURE 25. Accuracy of Section 3.2.3 regression model in estimating FI values for 12 shoulder cross sections images captured on BNSF track near Kansas City

3.4. IMAGING BASED BALLAST DEGRADATION ASSESSMENT FROM REGRESSION ANALYSIS

In total, 28 ballast cross section images at different degradation levels ranging from FI = 4 to FI = 46 were collected from different field sites within the scope of this research study. These include the 14 images collected from TTCI in Pueblo, Colorado, two images from SBC operation on UP track in Martinton, Illinois, and finally, the 12 images collected from BNSF track near Kansas City, Missouri. All of these images were processed using the developed image processing algorithm for the PDS index. As a final task, it was then decided to perform a statistical regression analysis on all the imaging data to establish a more comprehensive ballast degradation model relating FI to the PDS index.

Figure 26 shows the results of this analysis and the regression model achieved with a coefficient of determination R^2 equal to 0.84. Comparing this model with the one presented in Section 3.2.3 (Figure 19) shows that the correlation of the new model has improved by almost 9%. The new model once again confirms a strong linkage between FI and average PDS values. Therefore, this new regression model based on the image processing algorithm is established here as the final IDEA product of this research and can be used as an efficient tool for imaging based evaluation of ballast degradation levels for the machine vison system operating in the field.

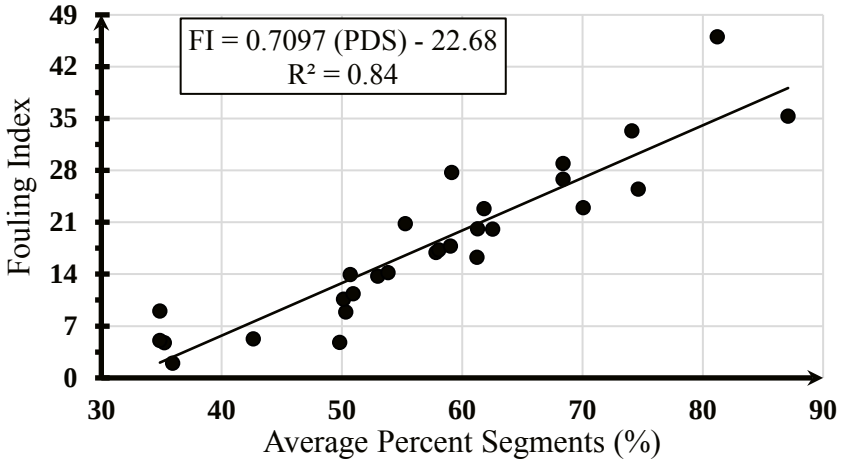

FIGURE 26. Imaging based ballast degradation model based on the complete database of 28 images of ballast cross sections collected from all the field experimentation sites in this research study

4. PLANS FOR IMPLEMENTATION

This IDEA research project developed machine vision tools for evaluating railroad ballast fouling conditions. When fully automated for everyday use, field inspectors and ballast maintenance personnel will be able to take advantage of the main research product, i.e. the ballast imaging kit and the segmentation approach, to quantify the level of ballast degradation from simple camera images of the ballast section in question. The approach applies computer vision algorithms and image processing techniques to process the collected images and compute a new image-based index Percent Degraded Segments (PDS), which has been linked to Selig's ballast Fouling Index (FI) commonly used by railroad practitioners for ballast condition assessment.

4.1. DEVELOPMENT OF BALLAST IMAGING AND EVALUATION KITS FOR TRACK INSPECTORS

The IDEA product developed in this study provides an immediate application for a simple portable method, or inspector's kit, which can be used in the field, called the Ballast Imaging Kit (BIK), shown in Figure 27, left and center. A single inspector can perform spot-checking of ballast degradation levels in suspected problem areas by quickly gathering quantifiable evidence through imaging, and then, process these images using the innovative PDS method to determine suitable maintenance and renewal decisions. A next step product will be the further development of the PDS technique into a user-independent image analysis software package. The conceptual Ballast Evaluation Kit (BEK), also shown in Figure 27 on the right, has been envisioned to run the proposed user-independent image analysis software on a laptop computer. This will enable the user to quantify ballast degradation levels using the BIK camera images taken on-site simultaneously. The BEK will contain all of the required items to perform an on-track evaluation and record the data, which can also be tagged with its Global Positioning System (GPS) location.

However, the method of spot-checking for ballast fouling assessment may miss the worst field conditions. It is more desirable to quantify the level of degradation along an entire stretch of track. An automated mobile platform with installed cameras and related shoulder cut section tools can accomplish that in the future. Both spatial variability of ballast fouling conditions and changes in ballast degradation linked to special trackwork and/or track transition zones, e.g., bridge approaches, can be objectively monitored in a consistent and automated fashion. To assist this process, a communications

plan needs to be established between FRA, railroads, and ballast maintenance teams through outreach, webinars, and trainings to inform all stakeholders about the benefits of such a continuous imaging-based ballast assessment alternative.

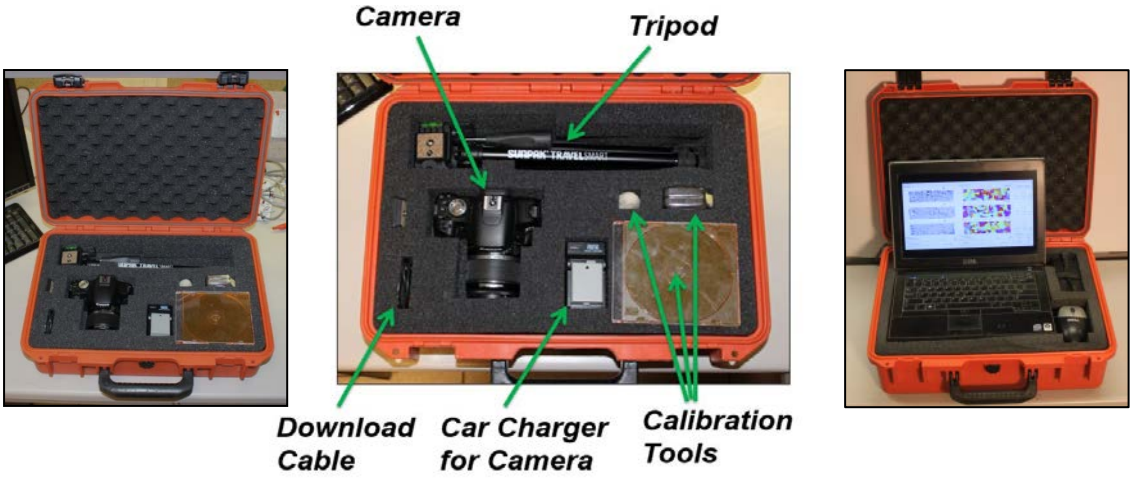

FIGURE 27. Ballast Imaging Kit (BIK) for practitioners and ballast inspectors to capture cross section images on-site (photo on the left and content description in the center); Ballast Evaluation Kit (BEK) to process images and quantify PDS (conceptual design on the right)

4.2. A MACHINE VISION SYSTEM FOR SHOULDER BALLAST CLEANERS

The integration of the BIK and BEK is envisioned as a future Machine Vision System for Shoulder Ballast Cleaners (MV-SBC), which will be applied over long sections of track to provide objective and continuous quantification of railroad ballast degradation levels. SBCs equipped with MV-SBC will expose cut-section views of ballast layers at desired depths to automate collection of ballast images from the shoulder of the track for evaluation using our PDS technique. We will incorporate a high-resolution camera, with a high-speed global shutter (for overcoming equipment vibration), to scan an 18-inch strip along the horizontal path of the cut section made by the SBC digging wheel. This will obtain the size and type of images we have used in our testing so far. A shroud would be included with an LED white light source to compensate for non-optimal environmental conditions (e.g., heavy dust conditions, direct sunlight or lack of illumination, etc.). We are investigating implementation methods with assistance from our project expert panel members from Loram Maintenance of Way and BNSF Railway.

We envision bringing BEK and MV-SBC developments into railroad practice in our future research efforts to offer the capability to quantify railroad ballast field conditions objectively, continuously and reliably without the need for periodic ballast bucket sampling and laboratory sieving. Routine application of the imaging-based technology will make it possible to frequently monitor ballast field deterioration levels over different periods at various locations along the track, including such areas as special trackwork and transition zones. Accordingly, SBCs equipped with MV-SBC can become continuous quantitative data collection devices for automated ballast condition monitoring and create a PDS database for a railroad company with GPS location data. Of course, this process could also be used to evaluate the effectiveness of ballast repair/renewal and other track substructure remediation activities. Overall, predictive modeling of heavy fouling, ballast service life, and ballast performance could be developed with the PDS data collected from the BEK and MV-SBC.

5. CONCLUSIONS

This research project introduces a machine vision-based inspection system for assessing ballast degradation levels using image analysis techniques and is applicable to both laboratory and field captured, cross section images. The approach in this project showed encouraging performance to successfully replace ballast bucket sampling and mechanical sieve analysis operations to assess the severity of ballast degradation. This technology was validated using ground truth data obtained from a wide range of ballast samples collected at different degradation levels from in-service track.

An image processing algorithm with three main modules including pre-processing, segmentation and post-processing was applied on the ballast cross section images collected in the laboratory and in the field. Field images of vertical (longitudinal and/or transverse to the track) and horizontal cut sections of in-service ballast were collected from different track locations. The ballast cross section images were analyzed to quantify different levels of ballast degradation from the images by the use of a newly introduced imaging-based index called Percent Degraded Segments (PDS). The PDS values from the field-collected images of ballast cut sections correlated well with the commonly used Selig's Fouling Index (FI) values obtained from sieve analysis results of the field collected ground truth samples. A color coding approach highlighting different sized particle images was found to be effective for the use of the image processing algorithm. A Graphical User Interface (GUI) supported the efficient determination of image segmentation parameters.

A procedure developed for acquiring images of both horizontal and vertical ballast cross sections in the laboratory and field was combined with an "image with corresponding sample" method for field ballast sampling. Capturing horizontal cross section images of ballast from the shoulder is a feasible approach for determining the condition of ballast at different depths and along extended stretches of track. These horizontal sections indicated similar degradation trends to those produced by Shoulder Ballast Cleaner (SBC) equipment during routine maintenance operations. As such, horizontal imaging of shoulder ballast cross sections showed promise to enable SBC equipment to obtain degradation quantification at desired cutting depths and therefore, identify an optimum depth of shoulder cleaning or undercutting to achieve targeted ballast maintenance goals for improved drainage and stability.

This study confirmed the need for collecting field images of in-service ballast cross sections for degradation assessment. It was found that reproducing vertical ballast cross sections in laboratory can be challenging. This may be attributed to the ballast layer moisture conditions contributing to maintain the arrangement of the particles in the field. Nevertheless, horizontal imaging of ballast cross sections in the field was found to be the preferred approach, and the developed laboratory ballast imaging tray technique can still be utilized to produce these in the laboratory. Therefore, this method can generate various degradation conditions, using a variety of customized samples containing specific combinations of degraded ballast particles sizes, to produce difficult to capture conditions in the field needed to expand the field-captured image database.

Regression analysis established a significant correlation between FI and average PDS values. Using 28 field cut section ballast images and their sieve analysis results in the laboratory, a simple linear relationship was found to exist between the FI and PDS values with a coefficient of determination (R^2) equal to 0.84. Accordingly, this imaging-based ballast degradation model was quite effective in estimating in-service ballast FI values, which typically ranged from 4 to 46, from the image processing algorithm PDS results.

The developed technology can quantify in-service ballast condition and its properties at any location, possibly identified by ground penetrating radar or other network condition monitoring devices, without the need for ballast sampling from trench cut sections. It can also be used with shoulder cleaning and undercutting equipment to automate the condition assessment using images of ballast cut sections below the ties. As such, this automated evaluation could greatly improve the quality and efficiency of ballast maintenance activities. In addition, the results of this process can be used for inspection purposes and to map out recommendations of follow-up rehabilitation strategies. Further, the proposed method has the potential to be applied for in-situ evaluation of permeability and strength properties of railroad ballast at different degradation levels.

REFERENCES

[1] E. T. Selig and J. M. Waters. *Track Geotechnology and Substructure*. London, Telford, 1994.
[2] C.C. Chiang. *Effects of Water and Fines on Ballast Performance in Box Tests*. Master of Science Degree Project Report No. AAR89-366P," University of Massachusetts, 1989.
[3] X. Han and E. T. Selig. Effects of Fouling on Ballast Settlement. In Proceedings of 6th International Heavy Haul Railway Conference, Cape Town, South Africa.
[4] A. Ebrahimi, J. M. Tinjum, T. B. Edil. Protocol for Testing Railway Ballast in Large Scale Cyclic Triaxial Equipment. ASTM Geotechnical Testing Journal, vol. 35, no. 5, pp. 762-804, 2012.
[5] M. Moaveni, S. Wang, J. M. Hart, E. Tutumluer and N. Ahuja, "Aggregate Size and Shape Evaluation Using Segmentation Techniques and Aggregate Image Processing Algorithms," Journal of Transportation Research Board, no. 2335, pp. 50-59, 2013.
[6] M. Moaveni, Y. Qian, I. Qamhia, E. Tutumluer, C. Basye, D. Li. Morphological Characterization of Railroad Ballast Degradation Trends in the Field and Laboratory. Transportation Research Record: Journal of the Transportation Research Board, vol. 2545, pp. 89-99, 2016.

[7] E. Tutumluer, S. Schmidt, I. Qamhia, I., C. Basye, D. Li, S. C. Douglas. Ballast Properties and Degradation Trends Affecting Strength, Deformation and In-Track Performance. In AREMA Annual Conference, Minneapolis, MN, 2015.
[8] D. Jobson, Z. Rahman, and G. Woodell. A Multiscale Retinex for Bridging the Gap between Color Images and the Human Observation of Scenes. IEEE Transactions on Image Processing, vol. 6, no. 7, 1997.
[9] R.C. Gonzalez, R. E. Woods, S. L. Eddins. *Digital Image Processing Using Matlab*. Tata McGraw Hill, 2010.
[10] E. Pisano, S. Zong, M. Hemminger, M. Deluca, R. Johnston, K. Muller, M. Braeuning, and S. Pizer. Contrast Limited Adaptive Histogram Equalization Image Processing to Improve the Detection of Simulated Speculations in Dense Mammograms. Journal of Digital Imaging, vol. 11, no. 4, pp. 193-200, 1998.
[11] S. Paris. Bilateral Filtering: Theory and Applications. Foundations and Trends in Computer Graphics and Vision, vol. 4, no. 1, pp. 1-73, 2008.
[12] L. Vincent and P. Soille. Watershed in Digital Spaces: An Efficient Algorithm Based on Immersion Simulation. IEEE Transactions on Pattern Analysis and Machine Intelligence, vol. 13, no. 6, 1991.
[13] *MATLAB and Statistics Toolbox Release 2015b*. Natick, Massachusetts: The MathWorks, Inc.
[14] K. N. Chaudhury, D. Sage, and M. Unser. Fast O(1) Bilateral Filtering Using Trigonometric Range Kernels. IEEE Trans. Image Processing, vol. 20, no. 11, 2011.
[15] M. de Berg, M. van Kreveld, M. Overmars, and O. Schwarzkopf. *Computational Geometry: Algorithms and Applications*. Springer, pp. 2-8, 2000.

APPENDIX I. PARTICLE SIZE DISTRIBUTION CURVES

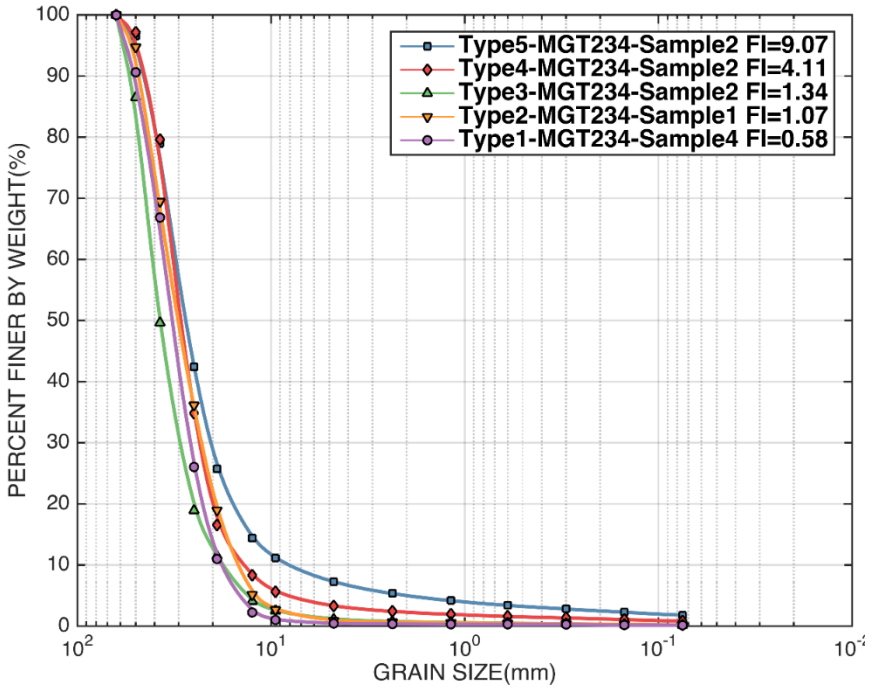

IA. Gradation curves and corresponding Selig's Fouling Indices (FI) for the 5 ballast types at approximately 234 MGT level collected from the UP ballast box study

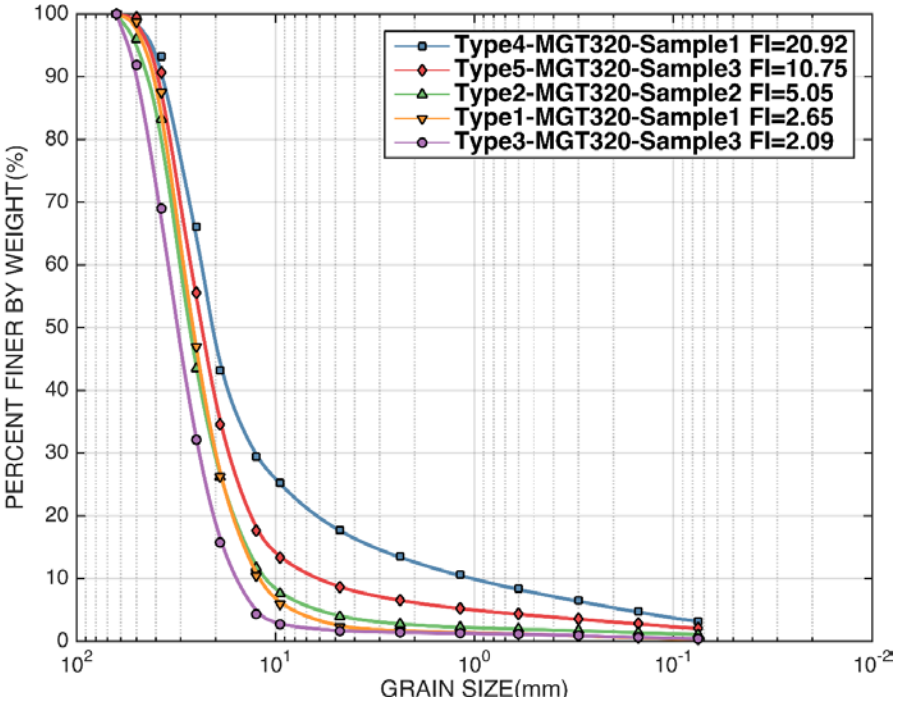

IB. Gradation curves and corresponding Selig's Fouling Indices (FI) for the 5 ballast types at approximately 320 MGT level collected from the UP ballast box study

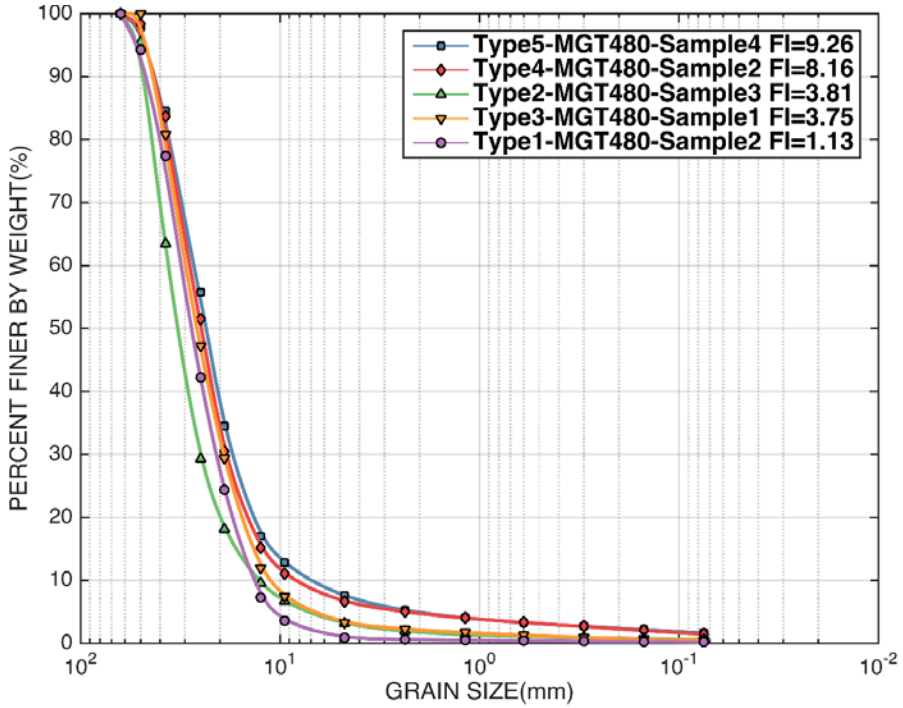

IC. Gradation curves and corresponding Selig's Fouling Indices (FI) for the 5 ballast types at approximately 480 MGT level collected from the UP ballast box study

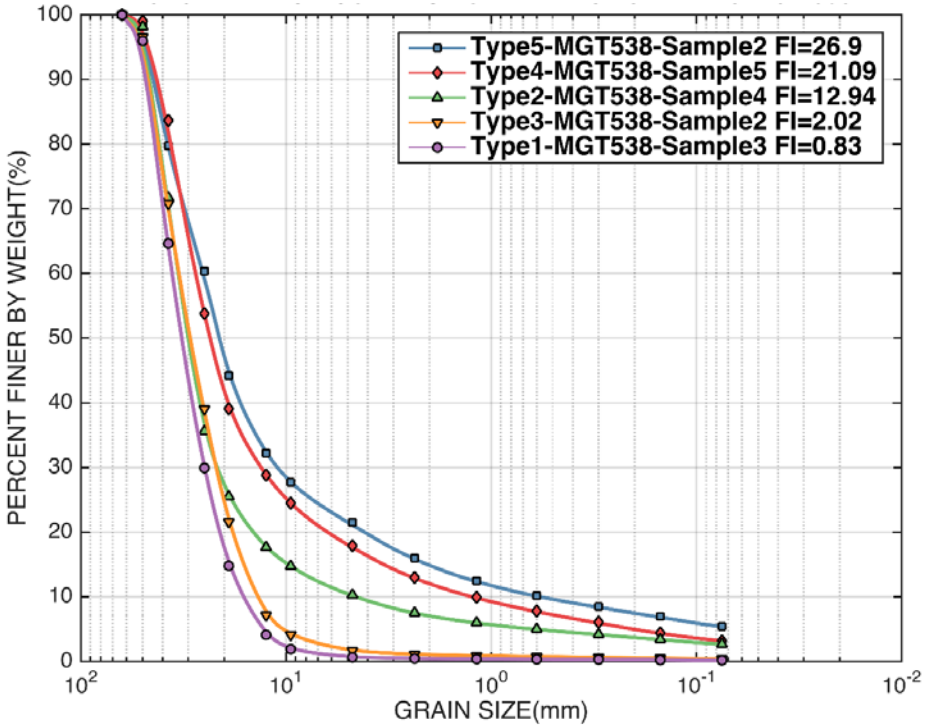

ID. Gradation curves and corresponding Selig's Fouling Indices (FI) for the 5 ballast types at approximately 538 MGT level collected from the UP ballast box stud

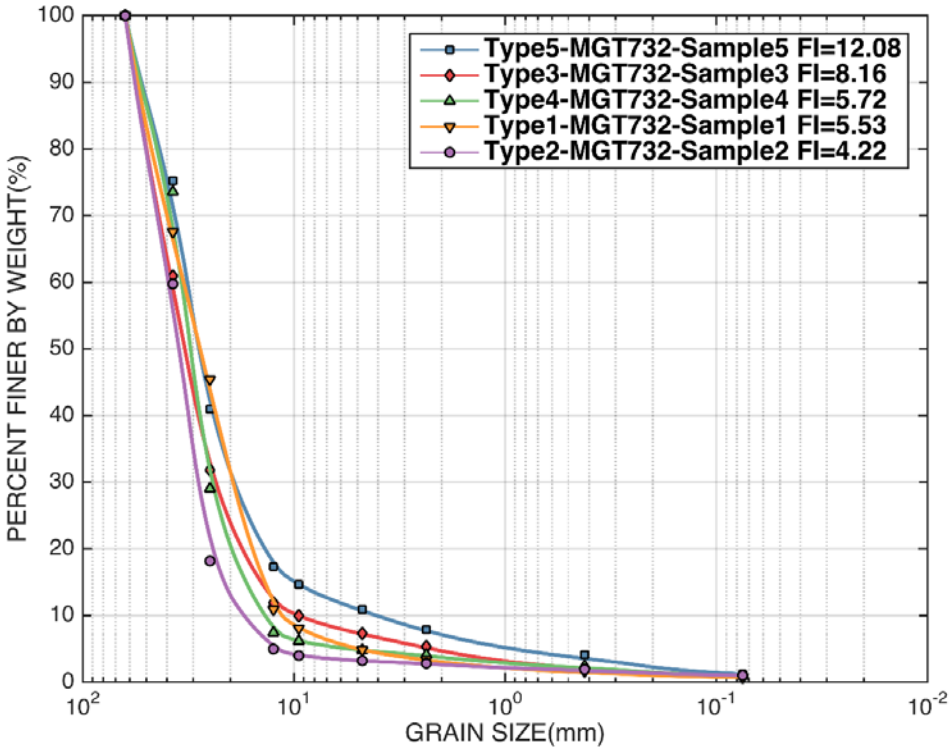

IE. Gradation curves and corresponding Selig's Fouling Indices (FI) for the 5 ballast types at approximately 732 MGT level collected from the UP ballast box study

APPENDIX II. LABORATORY BALLAST IMAGING

Ballast Imaging Experimentation with the Metal Box

A portable shop crane was used to lift and lower the metal sliding doors. Two buckets of quartzite ballast material ("Type 3" as shown in Table 1) collected at approximately 732 MGT traffic level with an FI value of 16 was used to fill the front side of the wooden divider. The ballast material was placed inside the box two times. In the first trial, the interior metal sliding door was lifted after filling the box and before capturing the cross-section image. Due to the thickness of the sliding door, the ballast particles moved slightly toward the Plexiglas wall while lifting the door. This small movement caused the fine material to further settle down at the bottom of the box. To improve this condition, it was decided to perform the second trial and fill the box without using the inside metal sliding door. It was observed that in each trial case, dry fine (dust-sized) particles tended to settle down at the bottom of the box due to gravity and the lifting of the door. Additionally, the dust generated while placing the ballast materials inside the box also blocked the view through the Plexiglas and prevented a clear sight of the ballast. A wooden divider was manufactured and placed inside the metal box to decrease the volume of the box so that even small quantities of field sampled ballast could be used to partially fill the box, for example, with only two 5-gallon buckets of ballast material to establish of ballast trench cut view of up to 21-in. (533 mm) height. The captured vertical cross section images of the ballast sample from the two trials (with and without the interior metal sliding door) are shown below.

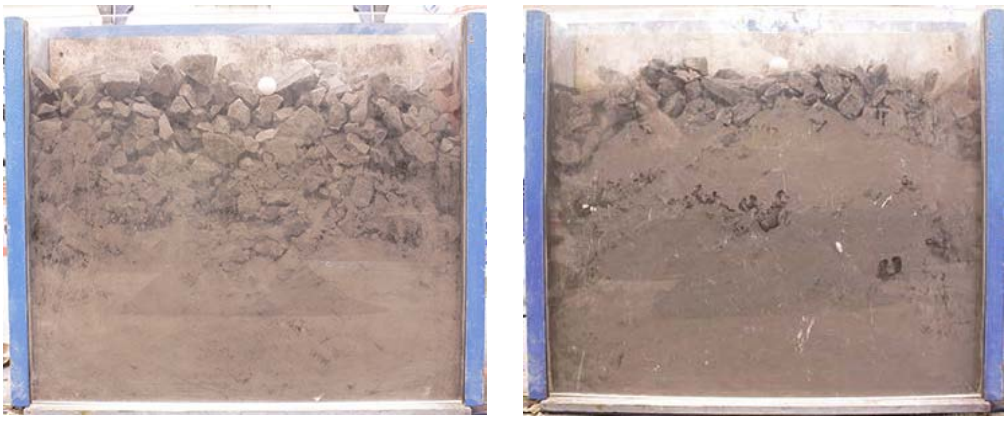

Figure IIA. Cross section images of Type 3 ballast sample (FI=16% at approximately 732 MGT level) captured with (left) and without (right) the use of interior metal sliding door

Procedure for Capturing Top View Images of Ballast in a Tray

The tray imaging started with pouring a bucket containing a field collected ballast sample onto the tray. Then, top view images were captured using the DSLR camera placed above the tray. Note that the tray had the capacity to carry the total bulk volume of a 5-gallon bucket full of ballast materials. Moreover, the plan view dimensions of the tray matched the required size and aspect ratio of the images captured for each sample. A laser-scan video could also be recorded during the plan view image acquisition process. Several laser-scan videos were acquired although it was beyond the scope of this study. The laser-scan video has the potential to be used later for developing algorithms to estimate ballast surface height profile/irregularities through machine learning techniques. The tray was designed with wheels that could ride on a track to allow sliding it forward during laser scan and image acquisition, then tipping it to empty the ballast back into the bucket. The top view images are presented below in Tables IIA to IIE.

Table IIA. Laboratory top view tray images of ballast types 1 to 5 at approximately 234 MGT level

Sample ID = 1-234-4 FI = 0.58				
				
Trial 1	*Trial 2*	*Trial 3*	*Trial 4*	*Trial 5*
Sample ID = 2-234-1 FI = 1.07				
				
Trial 1	*Trial 2*	*Trial 3*	*Trial 4*	*Trial 5*
Sample ID = 3-234-2 FI = 1.34				
				
Trial 1	*Trial 2*	*Trial 3*	*Trial 4*	*Trial 5*
Sample ID = 4-234-2 FI = 4.11				
				
Trial 1	*Trial 2*	*Trial 3*	*Trial 4*	*Trial 5*
Sample ID = 5-234-2 FI = 9.07				
				
Trial 1	*Trial 2*	*Trial 3*	*Trial 4*	*Trial 5*

Table IIB. Laboratory top view tray images of ballast types 1 to 5 at approximately 320 MGT level

Sample ID = 1-320-1 FI = 2.65				
				
Trial 1	*Trial 2*	*Trial 3*	*Trial 4*	*Trial 5*
Sample ID = 2-320-2 FI = 5.05				
				
Trial 1	*Trial 2*	*Trial 3*	*Trial 4*	*Trial 5*
Sample ID = 3-320-3 FI = 2.09				
				
Trial 1	*Trial 2*	*Trial 3*	*Trial 4*	*Trial 5*
Sample ID = 4-320-1 FI = 20.92				
				
Trial 1	*Trial 2*	*Trial 3*	*Trial 4*	*Trial 5*
Sample ID = 5-320-3 FI = 10.75				
				
Trial 1	*Trial 2*	*Trial 3*	*Trial 4*	*Trial 5*

Table IIC. Laboratory top view tray images of ballast types 1 to 5 at approximately 480

Sample ID = 1-480-2 FI = 1.13				
				
Trial 1	*Trial 2*	*Trial 3*	*Trial 4*	*Trial 5*
Sample ID = 2-480-3 FI = 3.81				
				
Trial 1	*Trial 2*	*Trial 3*	*Trial 4*	*Trial 5*
Sample ID = 3-480-1 FI = 3.75				
				
Trial 1	*Trial 2*	*Trial 3*	*Trial 4*	*Trial 5*
Sample ID = 4-480-2 FI = 8.16				
				
Trial 1	*Trial 2*	*Trial 3*	*Trial 4*	*Trial 5*
Sample ID = 5-480-4 FI = 9.26				
				
Trial 1	*Trial 2*	*Trial 3*	*Trial 4*	*Trial 5*

Table IID. Laboratory top view tray images of ballast types 1 to 5 at approximately 538 MGT level

Sample ID = 1-538-3 FI = 0.83				
				
Trial 1	*Trial 2*	*Trial 3*	*Trial 4*	*Trial 5*
Sample ID = 2-538-4 FI = 12.94				
				
Trial 1	*Trial 2*	*Trial 3*	*Trial 4*	*Trial 5*
Sample ID = 3-538-2 FI = 2.02				
				
Trial 1	*Trial 2*	*Trial 3*	*Trial 4*	*Trial 5*
Sample ID = 4-538-5 FI = 21.09				
				
Trial 1	*Trial 2*	*Trial 3*	*Trial 4*	*Trial 5*
Sample ID = 5-538-2 FI = 26.9				
				
Trial 1	*Trial 2*	*Trial 3*	*Trial 4*	*Trial 5*

Table IIE. Laboratory top view tray images of ballast types 1 to 5 at approximately 732 MGT level

Sample ID = 1-732-1 FI = 5.53				
				
Trial 1	*Trial 2*	*Trial 3*	*Trial 4*	*Trial 5*
Sample ID = 2-732-2 FI = 4.22				
				
Trial 1	*Trial 2*	*Trial 3*	*Trial 4*	*Trial 5*
Sample ID = 3-732-3 FI = 8.16				
				
Trial 1	*Trial 2*	*Trial 3*	*Trial 4*	*Trial 5*
Sample ID = 4-732-4 FI = 5.72				
				**N/A** *(raw image file corrupted)*
Trial 1	*Trial 2*	*Trial 3*	*Trial 4*	*Trial 5*
Sample ID = 5-732-5 FI = 12.08				
				
Trial 1	*Trial 2*	*Trial 3*	*Trial 4*	*Trial 5*

APPENDIX III. SEGMENTATION PARAMETERS AND PDS VALUES - TOP VIEW TRAY IMAGES

Table IIIA. Segmentation parameters and PDS values for top view tray images of ballast types 1 to 5 at approximately 234 MGT level

Sample ID	Imaging Trial	Size of 1-inch calibration ball considered in the analysis (pixels)	Average PDS (%)	Mean of Average PDS for Five Trials (%)	Std. Dev of Average PDS for Five Trials (%)
1-234-4	1	211	52.85	50.63	2.68
1-234-4	2	208	51.95		
1-234-4	3	208	46.19		
1-234-4	4	208	52.10		
1-234-4	5	208	50.08		
2-234-1	1	226	52.27	50.77	4.21
2-234-1	2	229	55.60		
2-234-1	3	220	44.24		
2-234-1	4	226	52.04		
2-234-1	5	223	49.68		
3-234-2	1	205	54.37	53.84	0.865
3-234-2	2	205	52.58		
3-234-2	3	202	54.54		
3-234-2	4	205	54.42		
3-234-2	5	202	53.29		
4-234-2	1	202	51.05	52.03	3.44
4-234-2	2	208	58.27		
4-234-2	3	208	48.69		
4-234-2	4	205	49.24		
4-234-2	5	199	52.21		
5-234-2	1	208	57.03	52.50	2.63
5-234-2	2	208	51.18		
5-234-2	3	217	50.29		
5-234-2	4	211	52.31		
5-234-2	5	208	51.67		

Table IIIB. Segmentation parameters and PDS values for top view tray images of ballast types 1 to 5 at approximately 320 MGT level

Sample ID	Imaging Trial	Size of 1-inch calibration ball considered in the analysis (pixels)	Average PDS (%)	Mean of Average PDS for Five Trials (%)	Std. Dev of Average PDS for Five Trials (%)
1-320-1	1	196	55.46	52.52	3.47
1-320-1	2	196	46.99		
1-320-1	3	190	53.74		
1-320-1	4	199	55.04		
1-320-1	5	190	51.40		
2-320-2	1	202	53.99	53.53	4.93
2-320-2	2	196	60.84		
2-320-2	3	193	49.86		
2-320-2	4	202	48.18		
2-320-2	5	199	54.78		
3-320-3	1	205	56.51	55.64	2.92
3-320-3	2	202	54.06		
3-320-3	3	205	51.73		
3-320-3	4	202	56.37		
3-320-3	5	205	59.54		
4-320-1	1	199	72.16	60.06	7.21
4-320-1	2	199	60		
4-320-1	3	202	54.53		
4-320-1	4	196	54.55		
4-320-1	5	196	59.04		
5-320-3	1	208	58.72	50.56	5.32
5-320-3	2	202	51.47		
5-320-3	3	202	51.04		
5-320-3	4	202	46.15		
5-320-3	5	208	45.44		

Table IIIC. Segmentation parameters and PDS values for top view tray images of ballast types 1 to 5 at approximately 480 MGT level

Sample ID	Imaging Trial	Size of 1-inch calibration ball considered in the analysis (pixels)	Average PDS (%)	Mean of Average PDS for Five Trials (%)	Std. Dev of Average PDS for Five Trials (%)
1-480-2	1	208	55.84	51.14	4.58
1-480-2	2	214	45.68		
1-480-2	3	205	53.71		
1-480-2	4	211	53.70		
1-480-2	5	211	46.76		
2-480-3	1	205	64.26	55.80	5.30
2-480-3	2	211	49.52		
2-480-3	3	208	54.76		
2-480-3	4	205	55.47		
2-480-3	5	214	55.00		
3-480-1	1	196	52.21	55.45	3.72
3-480-1	2	205	58.99		
3-480-1	3	196	51.84		
3-480-1	4	199	59.75		
3-480-1	5	196	54.45		
4-480-2	1	211	57.60	55.74	5.09
4-480-2	2	202	58.19		
4-480-2	3	205	55.03		
4-480-2	4	202	60.54		
4-480-2	5	208	47.33		
5-480-4	1	211	68.87	59.79	6.43
5-480-4	2	214	61.40		
5-480-4	3	208	60.64		
5-480-4	4	214	51.48		
5-480-4	5	211	56.53		

Table IIID. Segmentation parameters and PDS values for top view tray images of ballast types 1 to 5 at approximately 538 MGT level

Sample ID	Imaging Trial	Size of 1-inch calibration ball considered in the analysis (pixels)	Average PDS (%)	Mean of Average PDS for Five Trials (%)	Std. Dev of Average PDS for Five Trials (%)
1-538-3	1	213	52.27	50.95	2.56
1-538-3	2	216	53.46		
1-538-3	3	213	52.01		
1-538-3	4	216	46.90		
1-538-3	5	210	50.13		
2-538-4	1	208	72.66	61.20	7.33
2-538-4	2	208	64.03		
2-538-4	3	211	58.30		
2-538-4	4	214	54.39		
2-538-4	5	211	56.65		
3-538-2	1	211	48.75	50.37	2.55
3-538-2	2	208	46.70		
3-538-2	3	205	52.12		
3-538-2	4	208	52.76		
3-538-2	5	205	51.54		
4-538-5	1	208	65.99	67.41	4.91
4-538-5	2	205	69.55		
4-538-5	3	211	59.80		
4-538-5	4	211	68.84		
4-538-5	5	205	72.88		
5-538-2	1	211	78.18	68.49	6.00
5-538-2	2	211	62.21		
5-538-2	3	214	66.87		
5-538-2	4	208	69.40		
5-538-2	5	211	65.78		

Table IIIE. Segmentation parameters and PDS values for top view tray images of ballast types 1 to 5 at approximately 732 MGT level

Sample ID	Imaging Trial	Size of 1-inch calibration ball considered in the analysis (pixels)	Average PDS (%)	Mean of Average PDS for Five Trails (%)	Std. Dev of Average PDS for Five Trails (%)
1-732-1	1	210	50.63	52.78	4.59
1-732-1	2	213	50.23		
1-732-1	3	207	48.05		
1-732-1	4	216	55.70		
1-732-1	5	204	59.29		
2-732-2	1	226	51.07	50.50	3.08
2-732-2	2	229	54.84		
2-732-2	3	220	46.26		
2-732-2	4	226	50.72		
2-732-2	5	223	49.61		
3-732-3	1	211	42.92	45.30	2.19
3-732-3	2	208	45.65		
3-732-3	3	211	43.54		
3-732-3	4	214	48.48		
3-732-3	5	217	45.92		
4-732-4	1	214	51.38	51.73	2.01
4-732-4	2	220	54.14		
4-732-4	3	223	52.12		
4-732-4	4	217	49.26		
4-732-4	5	N/A	N/A		
5-732-5	1	211	55.19	50.87	3.01
5-732-5	2	220	53.33		
5-732-5	3	220	48.78		
5-732-5	4	211	47.77		
5-732-5	5	217	48.40		

APPENDIX IV. BALLAST CROSS SECTION IMAGES AND FOULING INDICES - HTL at TTCI

Procedure for Ballast Imaging in Trenches

A custom camera mounting system was used for consistent image acquisition of various sections of the trench walls. This was accomplished by attaching a 15.1-megapixel DSLR camera to a 3-DOF positioner at the end of a vertical bar. The bar was lowered into the trench and clamped to a horizontal bar secured at each end of the rails. The system was calibrated to position the camera for capturing images of a 24-in. (609 mm) by 16-in. (406 mm) section of the ballast cross section under the tie. The camera attachment was then unclamped and slid along the horizontal bar to image the next location with only limited recalibration. After each image was taken and before moving the camera, the borders of the camera's field of view were marked on the trench wall to identify the location for ballast sampling. Finally, the ballast material corresponding to the imaged area was carefully shaved off, using geologist's chisels, from the trench wall into a material handling tray and stored in 5-gallon buckets for sieve analysis. Collecting the ballast samples was conducted with extreme care in order to capture all particles and fines into the tray below.

Image capture was assisted by connecting the camera to a laptop running camera control software to view and capture the images remotely. This eliminated the need for personnel to be in the trench and allowed the camera to be placed up against the opposite wall, thus maximizing the field of view of the camera. The main considerations in capturing the images involved proper exposure, consistent spatial resolution and a reduction of any distortions of the ballast particles in the image. Adequate sunlight was cast evenly across the section for proper exposure but needed to be diffused in order not to cast shadows, in addition, a triple exposure setting was used to capture three consecutive images; the auto metered exposure and one image with a slightly lighter setting and the third with a slightly darker setting. This ensured that one or more field images would be suitable for processing since these images could not be retaken once the trench was refilled with ballast for continuing train operations. Captured ballast cross section images and corresponding fouling indices are presented in the table below.

Image ID = 5-1557-C2 FI = 8.87	Image ID = 1-1050-C2 FI = 10.6	Image ID = 1-1050-C1 FI = 11.34
		
Image ID = 4-1460-C2 FI = 13.71	**Image ID = 2-1308-C2 FI = 14.19**	**Image ID = 5-1557-C1 FI = 16.26**
		
Image ID = 2-1308-C1 FI = 16.9	**Image ID = 4-1460-C1 FI = 17.25**	**Image ID = 3-1354-C1-Wall2 FI = 17.78**
		
Image ID = 3-1396-C2 FI = 20.07	**Image ID = 3-1354-I1 FI = 20.11**	**Image ID = 3-1396-C1 FI = 20.79**
		
Image ID = 3-1354-C1 FI = 22.81		**Image ID = 3-1354-C2-Wall2 FI = 22.98**
		

APPENDIX V. SHOULDER SECTION IMAGES AND FOULING INDICES - BNSF, KANSAS CITY

Procedure for Shoulder Ballast Imaging

First, a mini-backhoe was used to dig down through the shoulder to a depth of 6-in. (152 mm) below the tie. After a horizontal shoulder cross section was exposed, three top view images with 24 in. (609 m) × 16 in. (406 mm) size at three different exposure levels were captured with a DSLR camera. The 1-in. (25.4 mm) ball was placed on the surface of the cross section for calibration purposes; during image processing, this calibration ball would help identify the spatial resolution of the image. Following optical imaging, a thermographic camera was used to capture the corresponding infrared image of the exposed shoulder cross section. This was part of a preliminary experiment to collect temperature signatures to study the level of degradation and moisture conditions of in-service ballast cross sections. A light diffuser was used at all stages to ensure uniform levels of natural light on the area of interest and prevent unwanted shadows in the image. After imaging, the ballast material corresponding to the imaged area was collected using chisels and mini-shovels and stored in 5-gallon buckets for future laboratory sieve analysis. Captured ballast cross section images and corresponding fouling indices are presented in the table below.

Image ID =75-76-77 **FI = 4.75**	**Image ID = 07-08-09** **FI = 4.79**	**Image ID = 39-40-41** **FI = 5.03**
		
Image ID = 78-79-80 **FI = 5.25**	**Image ID = 87-88-89** **FI = 13.94**	**Image ID = 50-51-52** **FI = 25.46**
	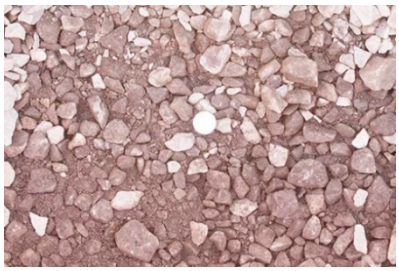	
Image ID = 34-35-36 **FI = 26.81**	**Image ID = 47-48-49** **FI = 27.73**	**Image ID = 38-39-40** **FI = 28.92**
	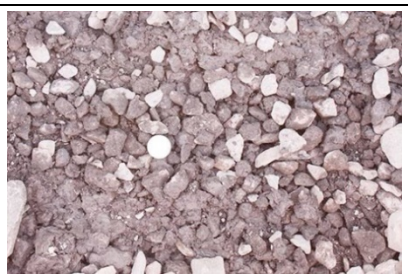	
Image ID = 81-82-83 **FI = 33.32**	**Image ID = 63-64-65** **FI = 35.30**	**Image ID = 20-21-22** **FI = 46.04**
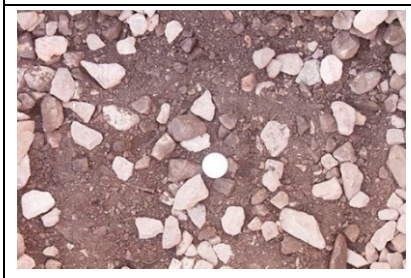	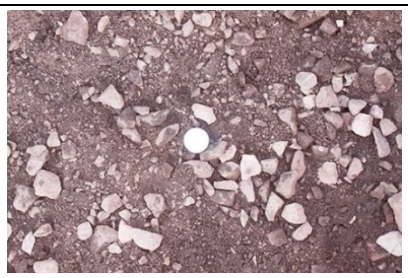	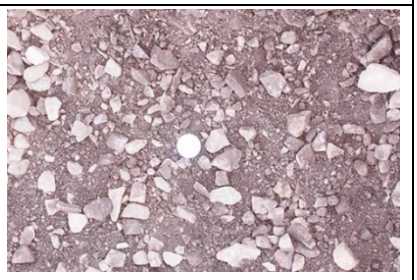

APPENDIX VI. RESPONSES TO COMMENTS FROM EXPERT REVIEW PANEL

1) If they are doing ballast cleaning already, don't they know they already have a problem?

Our proposed method can do efficient spot checking without ballast sampling to find problematic areas using our Ballast Evaluation Kit (BEK). In addition, Shoulder ballast cleaning (SBC) is considered as an initial maintenance stage. Therefore, our continuous evaluation approach can be useful to identify follow up and major maintenance alternatives in critical and heavily degraded areas. The above points were added to the executive summary of the report to address this comment

2) This equipment would be great for documenting the Fouling status prior to cleaning.

Agreed. This imaging based technology can also be used to quantify the effectiveness of SBC activities.

3) The wording in the text boxes in Figure 7 is messed up.

Corrected.

4) How much interaction is needed for the image processing? Is this a day of work or seconds? How many iterations are typically needed? What is the skill level or training of the user that is required? Could this be automated?

A trained user can do the processing in 2-3 minutes. The algorithm has only three sets of parameters. So, typically two or three iterations are required before achieving the desirable outcome. Less than an hour is needed to train a user and it might take a couple of hours for the user to practice and get more efficient. Based on our experience we have narrowed down the range of each segmentation parameter to a small set of common values. For a group of similar images, some parameters don't need to be changed. We believe through simple image processing techniques, we can evaluate the input image to detect characteristics that will help to make the parameter adjustment; therefore, the automation of the process will be possible.

5) Again, could the process be automated to reduce the variation in PDS?

Please refer to answer to comment #4 above. From the project's experience we believe that the algorithm is not sensitive to small variations in the parameters; therefore, the variation between the users should not be significant.

6) You may wish to add comment in Exec Summary or in sect 4 Plan; a comment that in addition to image collection during shoulder cleaning, a procedure to collect images at various spot locations prior to cleaning would be useful in developing cleaning programs, and secondly, spot image collection at derailment sites could be helpful in determining if ballast fouling might be contributing factor, and warrant fouled ballast sample collection for lab analysis to confirm image.

These are very good comments and in response; related findings and project insights were added to the Executive Summary section and plans for implementation were added to Section 4 of the report.

7) While the report does comment on both ballast moisture, and lighting as factors affecting image, both of these items may be key in why correlation to fouling index was not better, but more importantly it would be helpful to include comment/recommendation on how to take image (dry or wet ballast)(minimum or maximum light). In my field testing experience, the fouled ballast exposed by digging is often wet even in very dry arid locations, and often dries out very quickly in sun and wind. I favor developing a recommended practice for taking images such as distance from track center-line (perhaps at end of tie), depth below top of tie, lighting, etc. but this should be an industry developed recommended practice.

Our final results reported in Figure 27 presents a very promising and improved correlation of 0.84 compared with what was achieved in Figure 14 ($R^2 = 0.57$) and Figure 20 ($R^2 = 0.75$). We also made references to this point in the text. A brief description of the image acquisition process has been included in Sections 3.2.1 and 3.3.2 of the report. Moreover, a step-

by step guideline for field ballast imaging was also included in the Ballast Evaluation Kit (BEK) for practitioners and ballast inspectors.

8) You may have already caught the typo, but on pg 22 - should read "clean ballast hopper door".

Corrected. All references in the report were replaced by “clean ballast hopper door” terminology.

9) All of the 3rd Generation SBC's (SBC 18 - 33), and also SBC 17 and the 4th Gen cleaners - SBC 2401 & SBC 2402 on the CSX have a considerable distance between the digging wheels and the clean ballast hopper. Also BNSF has only our 3rd Gen machines in operation on their property. SBC 2nd Gen units with the close hopper door position include SBC 9 - 15. It is most likely in the long term, we will be transitioning to 3rd & 4th Gen units.

Thank you for sharing useful information. We are glad to hear it won’t be a problem in current and future generation of SBCs. We clarified and adequately emphasized this point in the report.

10) I do see the potential for also using with an Undercutter for evaluating the conditions at the bottom of the cut. With the UC 1201 Undercutter equipment, there is a considerable open distance between the cutter wheels and the clean ballast return area. Also, there is a considerable amount of time for capturing images, as the machine speed is approximately 0.2 - 0.4 mph.

Thank you for sharing this useful information. We will have further discussion with you regarding these points especially while working on the implementation phase of this project.

11) Also one question and maybe I missed it in the report, but what is the capability and limitations for capturing images on the move with very high speed photography?

The research team has experience in taking images of moving trains to inspect components in the images for defects. Although high speed imaging might not be required, there is possibility to incorporate a high resolution camera, with a high-speed global shutter, to scan an 18" strip along the horizontal path of the cut section made by the SBC digging wheel. This will obtain the same size and type of images we have used in our testing so far. A shroud would be included with an LED white light source to compensate for non-optimal environmental conditions (e.g., equipment vibration, heavy dust conditions, direct sunlight or lack of illumination) as needed. These will be further investigated at the implementation phase of this proposed technology.